










Article

Distinct B-Cell Specific Transcriptional Contexts of the BCL2 Oncogene Impact Pre-Malignant Development in Mouse Models

Lina Zawil ¹, Tiffany Marchiol ¹, Baptiste Brauge ², Alexis Saintamand ¹, Claire Carrion ¹, Elise Dessauge ², Christelle Oblet ¹, Sandrine Le Noir ¹, Frédéric Mourcin ², Mylène Brousse ¹, Paco Derouault ³, Mehdi Alizadeh ², Yolla El Makhour ⁴, Céline Monvoisin ², Julien Saint-Vanne ^{2,5}, Simon Léonard ^{2,6}, Stéphanie Durand-Panteix ¹, Karin Tarte ^{2,5,*} and Michel Cogne ^{1,2,5,*}

- ¹ Immunology Department, Faculty of Medicine, Limoges University, Cnrs Umr 7276, Inserm U1262, 2 Rue du Dr Marcland, 87000 Limoges, France
- ² UMR U 1236, Univ Rennes 1, INSERM, EFS Bretagne, Equipe Labellisée Ligue Contre le Cancer, 35000 Rennes, France
- ³ Chu Dupuytren, 87000 Limoges, France
- ⁴ Immunology Department, Science Faculty, Lebanese University, Beirut P.O. Box 6573/14, Lebanon
- ⁵ Siti Laboratory, Chu Rennes, 35000 Rennes, France
- ⁶ LabEx IGO “Immunotherapy, Graft, Oncology”, 44000 Nantes, France
- * Correspondence: karin.tarte@univ-rennes1.fr (K.T.); michel.cogne@inserm.fr (M.C.)



Citation: Zawil, L.; Marchiol, T.; Brauge, B.; Saintamand, A.; Carrion, C.; Dessauge, E.; Oblet, C.; Le Noir, S.; Mourcin, F.; Brousse, M.; et al. Distinct B-Cell Specific Transcriptional Contexts of the BCL2 Oncogene Impact Pre-Malignant Development in Mouse Models. *Cancers* **2022**, *14*, 5337. <https://doi.org/10.3390/cancers14215337>

Academic Editor: Aldo M. Roccaro

Received: 24 September 2022

Accepted: 21 October 2022

Published: 29 October 2022

Publisher’s Note: MDPI stays neutral with regard to jurisdictional claims in published maps and institutional affiliations.



Copyright: © 2022 by the authors. Licensee MDPI, Basel, Switzerland. This article is an open access article distributed under the terms and conditions of the Creative Commons Attribution (CC BY) license (<https://creativecommons.org/licenses/by/4.0/>).

Simple Summary: Beyond the classical t(14;18) translocation associated with follicular lymphoma, *BCL2* is deregulated in multiple B-cell malignancies, including some cases of myeloma, and through diverse genetic anomalies. It is currently unclear how the various deregulation patterns mechanistically impact the phenotype of these malignancies. We designed two different *BCL2* deregulation models in transgenic mice, whereby the oncogene was either associated with the IgH3’RR superenhancer, as in t(14;18), or inserted into the kappa light chain locus. We compared the impact of these models on B-cell fate and lymphoid tissues. Linkage to the IgH superenhancer showed a quite specific impact on germinal center B cell populations. The Ig kappa model was much less specific and strongly boosted the plasma cell in-flow and the accumulation of long-lived plasma cells.

Abstract: Upregulated expression of the anti-apoptotic *BCL2* oncogene is a common feature of various types of B-cell malignancies, from lymphoma to leukemia or myeloma. It is currently unclear how the various patterns of deregulation observed in pathology eventually impact the phenotype of malignant B cells and their microenvironment. Follicular lymphoma (FL) is the most common non-Hodgkin lymphoma arising from malignant germinal center (GC) B-cells, and its major hallmark is the t(14;18) translocation occurring in B cell progenitors and placing the *BCL2* gene under the control of the immunoglobulin heavy chain locus regulatory region (IgH 3’RR), thus exposing it to constitutive expression and hypermutation. Translocation of *BCL2* onto Ig light chain genes, *BCL2* gene amplification, and other mechanisms yielding *BCL2* over-expression are, in contrast, rare in FL and rather promote other types of B-cell lymphoma, leukemia, or multiple myeloma. In order to assess the impact of distinct *BCL2* deregulation patterns on B-cell fate, two mouse models were designed that associated *BCL2* and its full P1-P2 promoter region to either the IgH 3’RR, within a “3’RR-*BCL2*” transgene mimicking the situation seen in FL, or an Ig light chain locus context, through knock-in insertion at the Igk locus (“Igk-*BCL2*” model). While linkage to the IgH 3’ RR mostly yielded expression in GC B-cells, the Igk-driven up-regulation culminated in plasmablasts and plasma cells, boosting the plasma cell in-flow and the accumulation of long-lived plasma cells. These data demonstrate that the timing and level of *BCL2* deregulation are crucial for the behavior of B cells inside GC, an observation that could strongly impact the lymphomagenesis process triggered by secondary genetic hits.

Keywords: oncogene deregulation; translocation; lymphoma; plasmacytosis; germinal center

1. Introduction

Follicular lymphoma (FL) is the most frequent indolent non-Hodgkin's lymphoma (NHL), representing about 25% of B-cell malignancies [1]. This germinal center (GC) B-cell malignancy results from the malignant and clonal accumulation of centrocytes and follows a multistep lymphomagenesis process evolving over decades before clinical manifestations. After a long premalignant phase, the clinical course is slow and characterized by multiple relapses associated with increased resistance to therapy. Over time, approximately 30% of FL cases transform into aggressive diffuse large B-cell lymphoma (DLBCL).

The major FL genetic hallmark is the t(14;18) (q32, q21) translocation, which is found in 90% of FL cases and deregulates the anti-apoptotic gene *BCL2* by displacing it under the control of immunoglobulin (Ig) heavy chain locus regulatory elements. A less frequent translocation, t(3;14), involves *BCL6* and hereby indirectly deregulates *BCL2* [2]. Contrasting to *MYC* in Burkitt lymphoma, for which variant translocations onto Ig light chain loci are common, *BCL2* t(2;18) and t(18;22) variant translocations to light chain genes are rare in FL but found in 9% of chronic lymphocytic leukemia cases [3,4]. In addition to translocations, chromosomal amplification of *BCL2* is also observed in DLBCL and in mantle cell lymphoma [5]. The diverse patterns of *BCL2* deregulation are thus likely impacting the phenotype of *BCL2*-driven lymphoproliferative disorders.

The t(14;18) translocation stands as an aberrant V(D)J recombination product, joining double-strand breaks (DSBs) induced by RAG both in the IgH JH region (at position 14q32) and close to *BCL2* oncogene (at position 18q21) and hereby imposing an IgH-like pattern on *BCL2* gene accessibility and transcription [6]. *BCL2* is a transmembrane mitochondrial protein with dual roles, both inhibiting apoptosis and cell cycle entry. In mature B cells, expression of the IgH-translocated *BCL2* gene is mostly under the control of the transcriptional enhancers from the IgH locus 3' regulatory region (3'RR), which are the main locus drivers at mature B-cell stages [7]. These enhancers notably ensure accessibility of the locus to class switch recombination (CSR), somatic hypermutation (SHM), and hypertranscription in activated B cells and plasma cells (PCs) [7–10]. The functional result of this translocation is the imbalance between cell survival and death at a stage where mature B cells are intensely exposed to affinity-based selection within the GC. Normal GC B-cells are indeed prone to undergo cell death unless they are positively selected and induced to enter the memory B cell or the plasma cell compartments [11,12].

BCL2 is normally repressed in the GC to ensure the selection of high-affinity B cells, while apoptosis is promoted by proteins such as BAK, BAX, and BAD. *BCL2* deregulation yielded by t(14;18) thus jeopardizes the GC B cell survival checkpoint, and *BCL2* gene translocation stands as an early driver hit initiating lymphomagenesis in FL. Among naive B cells that have left the bone marrow (BM) and are circulating in the periphery, those harboring the t(14;18) translocation display a selective advantage during the GC reaction allowing them to persist as atypical memory B cells already carrying features of FL-like cells (FLLCs). Upon future Ag encounter, these premalignant FLLCs are prone to re-enter the GC and undergo additional SHM, with eventual additional oncogenic hits, under the iterative exposure to activation-induced deaminase (AID) [13–15]. Although an early and crucial anomaly marking pre-malignant B-cells, the t(14;18) is frequent in healthy adults and is not by itself sufficient for FL development, so the prevalence of FL does not exceed 0.03%. Among the most frequent additional hits, alterations of histone/chromatin modifying enzymes, including KMT2D, CREBBP, EZH2, and multiple linker-histone H1 family members, are collectively found in almost 100% of FL cases. Additional mutations, such as loss-of-function mutations of HVEM/TNFRSF14 or the introduction of N-glycosylation sites within Ig variable regions, have been shown to affect the crosstalk between tumor B cells and their surrounding microenvironment [15–18].

Exploring the mechanisms of such complex and multifactorial B-cell malignancies requires studying whole living organisms and has prompted the generation of several models in mice. Initial transgenic mouse models in which *BCL2* expression was driven by the $E\mu$ enhancer have mostly resulted in a polyclonal expansion of all B-cell compartments overexpressing *BCL2*, from progenitors to plasma cells [19,20]. Lymphoma development was reported mostly when the *BCL2* deregulation was associated with other spontaneously selected or experimentally enforced genetic anomalies, notably involving *Myc* [21,22]. However, lymphoproliferation observed in such conditions rather involved immature B cells and did not provide models for post-GC low-grade human lymphoma. Strikingly, the most widely used transgenic mice considered as a pertinent model of human FL and based on the tumorigenic potential of *BCL2* have been the *vavP-BCL2* transgenics, although they broadly overexpress *BCL2* in all hematopoietic lineages, including T cells and thus do not recapitulate the natural story of human FL where *BCL2* overexpression is restricted to mature B cells [23,24].

Therefore, in an aim to better understand the complex development of B-cell malignancies and the impact of B-cell specific *BCL2* deregulation, our current study explored two new mouse models, designed either for pan-B cell expression through a knock-in of *BCL2* in the *Igk* locus or for specific targeting of activated B-cells and GC-B cells with a *BCL2* transgene driven by the *IgH* 3'RR enhancers. Since the 3'RR is a major driver of the *IgH* locus remodeling in the GC, the latter model is expected to mimic the *BCL2* deregulation associated with FL more specifically. The *BCL2* promoter region has a characteristic structure comprising the P1 and P2 promoters, with P1 dominating normal lymphocytes, while a shift from P1 to P2 usage is observed in FL, in association with a strong increase in *BCL2* expression within the GC. Contrary to previously reported *BCL2* transgenes, we thus included the full human *BCL2* promoter region in our *BCL2* gene cassettes. Indeed, this region includes transcription factor-binding sites, notably for the repressor *BCL6* limiting *BCL2* transcription in normal GC cells [25]. The design of our constructs thus also aims at evaluating in mice the deregulation and the eventual mutations of the *BCL2* promoter region documented in patients.

On their own, both of our new mouse models promote mature B-cell expansion, but they, however, differ in terms of stage-specificity according to the context of *BCL2* deregulation, with 3'RR-*BCL2* mice showing the most GC-restricted phenotype. These models are pertinent for studying a pre-malignant stage in young mice, notably showing the impact of GC B-cell expansion on the other components of lymphoid tissues.

2. Materials and Methods

2.1. Cell Lines and Mouse Models

DoHH2, SU-DHL-4, SU-DHL-6, and OCI-Ly3 cell lines (Germinal center or activated B cell type Diffuse large B cell lymphoma (DLBCL)) were grown in RPMI 1640 medium supplemented with 10% Fetal calf serum (Dutscher, Catalog number: S1810-500) at 37 °C with 5% CO₂ atmosphere).

All in vivo experiments were performed in accordance with animal ethical rules, and all protocols were authorized by the French Ministry of Research according to European Union regulations (APAFiS 13900). All mice were bred in a specific and opportunistic-free (SOPF) animal facility.

Two new mouse models were designed for this study (Figure 1A):

1. The “3'RR-*BCL2*” model, with random integration of a transgene that contains a human *BCL2* gene cassette driven by the *BCL2* P1/P2 promoter region, under the control of the 3' *IgH* superenhancer (under the form previously described as a functional “core 3'RR” [26], combining the various enhancer elements from the *Ig* heavy chain locus 3' regulatory region, but devoid of the large intervening sequences located in-between enhancers in the mouse *IgH* locus);

2. The “Igκ-*BCL2*” model, in which the Jκ region is deleted and replaced with the same above-mentioned *BCL2* cassette [P1/P2 promoter *BCL2* gene], as a knock-in in the mouse Igκ light chain locus, immediately upstream of the Eκ enhancer.

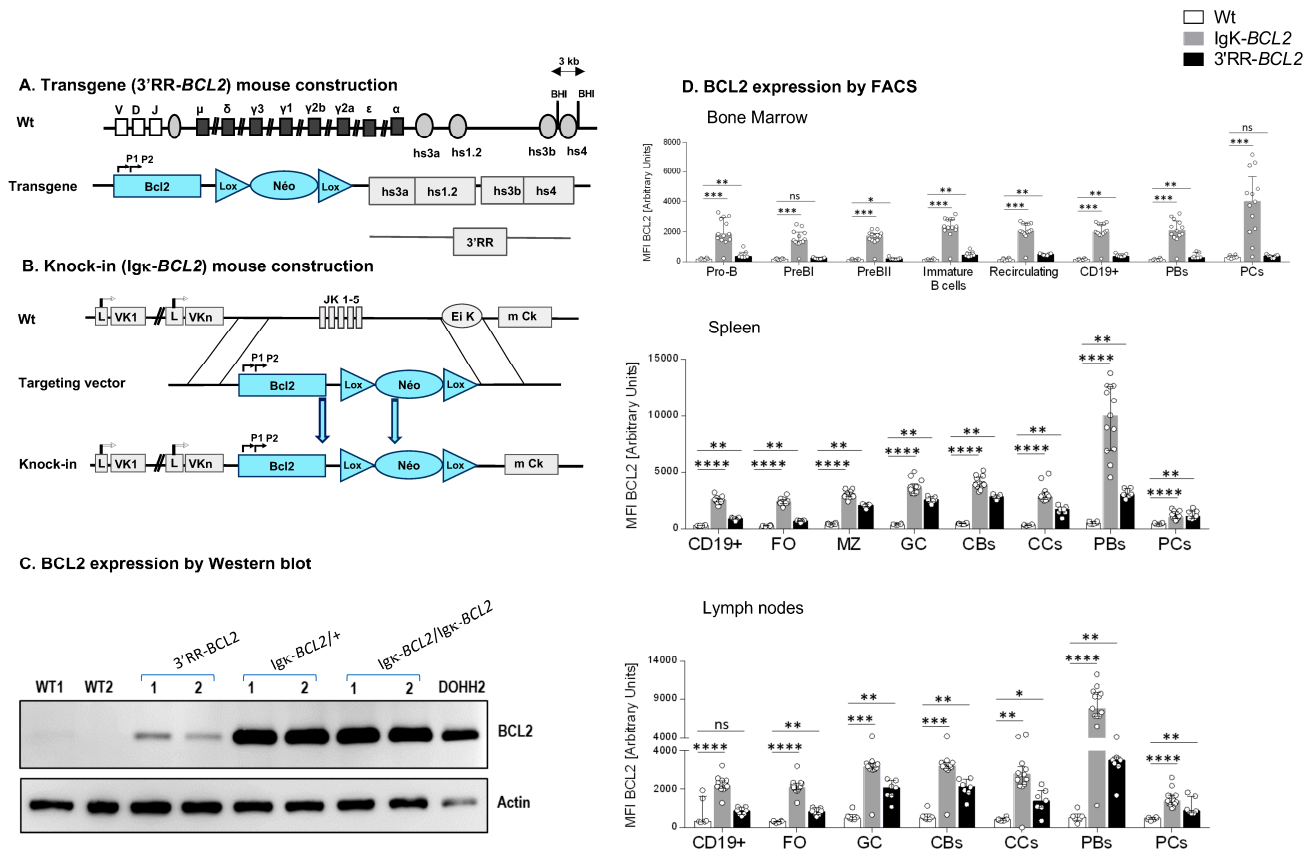


Figure 1. Mouse model construction schematics for (A) 3'RR-*BCL2* transgenics and (B) Igκ-*BCL2* knock-in mice. (C) Western-blot evaluation of human *BCL2* protein expression in the spleen of WT (negative control), 3'RR-*BCL2*, Igκ-*BCL2* Δ/+, Igκ-*BCL2* Δ/Δ mice, and in the DoHH2 human cell line (positive control). (D) Human *BCL2* expression in both mouse models, using the mean fluorescent intensity (MFI) obtained by flow cytometry from bone marrow, spleen, and mesenteric lymph nodes B-cells from unimmunized 3'RR-*BCL2* and Igκ-*BCL2* Δ/+, only. (* $p < 0.05$; ** $p < 0.01$; *** $p < 0.001$; **** $p < 0.0001$).

Both models thus contain the full promoter region of *BCL2*, including its two alternative promoters, P1 and P2, all in a mixed B6/129 genetic background.

2.2. Tumor Follow Up

A cohort of 19 Igκ-*BCL2* mice (12 homozygous and 7 heterozygous) and 8 3'RR-*BCL2* mice were monitored for the spontaneous development of tumors with time.

2.3. Flow Cytometry Analysis of Lymphoid Compartment

Single-cell suspensions from the BM and secondary lymphoid organs (spleen and mesenteric lymph nodes) were taken from mice that were either resting (unimmunized) or immunized with 3 iterative monthly SRBC injections. These cell suspensions were then labeled using various extracellular antibodies designed to identify the different early and late B-cell populations as well as the different T-cell populations in each of the organs mentioned above. Following the extracellular staining step, cells were fixed and permeabilized using the eBioscience FOXP3/transcription staining buffer set (Invitrogen, Reference: 00-5523-00) and then stained for intracellular proteins. The detailed list of antibodies used

in each of these panels is summarized in Supplementary Table S1. Cells were then analyzed by flow cytometry using an LSR FORTRESSA cytometer (Beckton Dickinson), and data analysis was performed using the Flow Logic system (the precise gating strategies for the different panels are listed in Supplementary Figure S1A–C).

Percentages were determined (for the different B cell sub-populations among CD19⁺ cells and for the different T cell sub-populations among CD4⁺ cells) as well as absolute cell numbers only in immunized mice (calculated based on the measured cell counts and lymphocyte percentages in the organ analyzed).

The mice used for evaluating lymphoid compartments represented 2 cohorts:

1. Resting cohort: this cohort comprising 6 wildtype, 13 hemizygous Igκ-*BCL2*/+, and 7 3'RR-*BCL2* mice was analyzed to carry out full characterizations of mice at the resting state;
2. Iteratively immunized cohort: 3 groups of 13 wildtype, 7 Igκ-*BCL2*/+, and 10 3'RR-*BCL2* mice were immunized intra-peritoneally at 3 months of age with 200 μL of Sheep Red Blood Cells (SRBC) and then iteratively over 3 consecutive months; they were sacrificed one month after the third immunization.

2.4. Western Blots

For the detection of human BCL2, we used wildtype mice as negative controls and the FL DoHH2 cell line as a positive control. Analyzed mouse samples included samples from transgenic (3'RR-*BCL2*) mice and from both homozygous (Igκ-*BCL2*/Igκ-*BCL2*) and hemizygous (Igκ-*BCL2*/+) Igκ knock-in mice.

A amount of 10 μg of total proteins were extracted (using 2× Laemmli buffer, Biorad, Catalog number # 161-0737, Composition: 65.8 mM Tris-HCl PH 6.8, 26.3% (*w/v*) glycerol, 2.1% SDS, 0.01% bromophenol blue) and denatured/reduced using β-mercaptoethanol (2.5% final) at 95 °C for 5 min.

After electrophoresis on a 12% polyacrylamide gel (Biorad, Hercules, CA, USA), proteins were transferred onto PVDF membranes (GE Healthcare). The human BCL2 protein was detected using the same mouse anti-human BCL2 antibody we use for flow cytometry, followed by an HRP-linked anti-mouse Ig antibody (eBioscience, San Diego, CA, USA), #18-8817-30).

Actin was stained as a housekeeping control protein with rabbit anti-actin antiserum (Sigma-Aldrich, Saint-Quentin, France A2066) followed by goat anti-rabbit-HRP (Southern Biotech, Birmingham, AL, USA, 4050-05).

Membranes were developed by enhanced chemiluminescence for a high-sensitivity detection system according to the manufacturer's instructions (Bio-Rad, Marnes-la-Coquette, France).

2.5. Proliferation Test

A separate cohort of 6 wildtype (WT), 4 Igκ-*BCL2*/+ hemizygous mice, and 5 3'RR-*BCL2* mice were injected intraperitoneally with 200 μL of SRBC at day 0, followed by another intraperitoneal injection with 200 μL of 5-ethynyl-2'-deoxyuridine (EdU) at Day 6, and they were sacrificed at day 7.

Single-cell suspensions were taken from the BM, spleen, and mesenteric lymph nodes and stained using the same panel described above but modified to be able to see the EDU⁺ cells. This was performed following the "Click-iT EdU Flow Cytometry Assay Kit protocol" (Molecular probes by Life Technologies, catalog numbers C10419, C10420). Cells were then analyzed by flow cytometry using the BD LSR FORTRESSA, and the data analysis was performed using the Flow Logic system.

2.6. Quantification of Antibody Affinity

We followed the indirect enzyme-linked immunosorbent assay (ELISA) described by Zhang et al. to quantify the affinity of the produced antibodies (notably IgG) in our mouse models compared to wildtype.

Mice were injected with Ovalbumin (Ova) at 1 ng/mL and Addavax (equal volume for both) on Day 0 and Day 14. Sera were taken on day 28, and quantification of total IgG in the serum was first performed, followed by the ELISA-based affinity study. Briefly, 96-well plates were coated with Ova at 2 µg/mL. Day 28 sera at a fixed concentration of 5×10^{-10} M were incubated overnight with Ova at different concentrations but always in large excess compared to IgG (4×10^{-7} to 6.25×10^{-9} M). The next day, the mix of serum IgG/Ova was incubated in 96-well plates previously coated with Ova at 2 µg/mL overnight. Then, the alkaline phosphatase-conjugated secondary antibody (anti-Mouse IgG) was added. After 45 min of incubation, P-Nitrophenyl phosphate (1 mg/mL) was added, alkaline phosphatase activity was blocked with 3 M Sodium hydroxide (NaOH), and the optical density was measured at 405 nm using a Multiskan FC photometer.

Finally, the dissociation constant (K_D) was evaluated by measuring the slope of the linear dependence [27].

2.7. Next-Generation Sequencing for Ig Repertoire Analysis and Global RNA Expression

We performed Ig repertoire sequencing analysis on RNA (500 ng–1.5 mg) extracted from:

1. BM, spleen, and mesenteric LNs from the iteratively immunized cohorts, including 3 groups of non-tumoral mice: wildtype (9 mice), Igκ-BCL2/+ (5 mice), and 3'RR-BCL2 (5 mice);
2. Spleen, mesenteric LNs, and tumoral tissues from mice affected with tumors, including 8 Igκ-BCL2 knock-in mice (5 Igκ-BCL2 homozygous + 3 hemizygous), and the single 3'RR-BCL2 transgenic mouse that developed lymphoma.

Repertoire sequencing was performed using RACE-PCR and high-throughput sequencing for determining cell repertoire diversity and the distribution of IgH clonotypes as previously described [28]. These experiments used a new generation methodology, which combines 5' RACE PCR; sequencing; and, for analysis, the international ImMunoGeneTics information system (IMGT), IMGT/HighV-QUEST Web portal, and IMGT-ONTOLOGY concepts. Briefly, we amplified IgH transcripts with 5' RACE PCR using a reverse primer. First, a mix containing up to 1 µg of RNAs, 1 µL of reverse primers hybridizing within the Ig µ (µ) and gamma (γ) CH1 exons, and dNTP mix was incubated 3 min at 72 °C and 2 min at 42 °C. After a short spin, the mix was placed on ice for 2 min, and 1 µL of ProtoScriptII enzyme (New England Biolabs) was added, together with a cap-race primer (5' AAGCAGTGGTATCAACGCAGAGTACAT[GGGG] 3', where the 4 G between brackets are ribonucleotides). The resulting cDNA was amplified with Taq Phusion (New England Biolabs) using a universal forward primer mix (5' CTAATACGACTCACTATAGGGC 3' and 5' CTAATACGACTCACTATAGGGCAAGCAGTGGTATCAACGCAGAGT 3', in a ratio of 4:1), as described [16], and a mix of reverse primers hybridizing within the µ and γ CH1 exons. Cycling conditions were 30 s at 98 °C, 32 cycles of 30 sec at 98 °C, 30 s at 65 °C, 30 s at 72 °C, and final elongation 5 min at 72 °C. Illumina sequencing adapters and tag sequences were then added by primer extension using Taq Phusion. Cycling conditions were 30 s at 98 °C, 12 cycles of 30 sec at 98 °C, 30 sec at 65 °C, 30 sec at 72 °C, and final elongation 5 min at 72 °C. The resulting amplicons were sequenced on an Illumina MiSeq sequencing system using MiSeq Reagent kit V3 500 cycles. Paired reads were merged using FLASH [29]. Repertoire analysis was performed using IMGT/HIGHV-QUEST tool (<http://imgt.org/>; accessed on 17 October 2021) [30] and associated RStudio package scripts; associated tools are available on the IMGT Web site.

Global evaluation of transcriptomic profiles was obtained using RNA-seq on lymphoid tissue samples (spleen and mesenteric lymph nodes) from the non-tumoral, iteratively immunized cohort, comparing samples from animals with three different genotypes, either wildtype, Igκ-BCL2/+, or 3'RR-BCL2. Sequencing was performed on an Illumina MiSeq, in a 2 × 150 bp configuration. Read counts from RNAseq normalized using the featureCount script were compared with DESeq2 (version 1.26.0) for evaluating differential expression along the binomial negative distribution. The results provided by DESeq2 were then submitted to variance stabilizing transformation [31]. A matrix of normalized values

restricted to genes with expression significantly modified ($p < 0.01$) in at least one genotype was then used in order to draw a heatmap of significantly modified signatures of interest using the “ggplot2” R package.

2.8. Single Cell Sequencing and Analysis

Three sets of 10-day splenic B cells were magnetically sorted (B cell negative selection kit, StemCell, Vancouver, Canada) from mice immunized once with SRBC. Single cells were captured and barcoded using the $10\times 3'$ sequencing kit (Chromium Next Gem Single cell $3'$ reagent kit v3.1, $10\times$ Genomics, Pleasanton, Ca, USA), and libraries were prepared following the manufacturer's instructions. Libraries were run using 2×75 paired-end reads on the HiSeq4000 Illumina sequencer. Raw data were successively processed and analyzed with the $10\times$ Cell Ranger ($10\times$ Genomics, Pleasanton, Ca, USA) and Seurat (v3.2.3) package [32]. Mean reads per cell were 40,766 for the WT sample, 66,971 for the $3'$ RR-BCL2 sample, and 102,596 for the $Ig\kappa$ -BCL2 sample. Median genes per cell over 3 samples varied from 1767 to 1869. Cells expressing less than 800 or more than 4500 genes or with more than 20,000 unique molecular identifiers (umi) counts were filtered out. Cells with a frequency of mitochondrial genes of more than 8% or with a frequency of ribosome genes of less than 10% were also removed from the analysis. Contaminating T cells and myeloid cells were detected based on canonical markers (Cd3 genes and C1q genes) and filtered out. Gene counts were normalized using the SCTransform package (v0.3.1) with a second non-regularized linear regression applied to the percentage of mitochondrial and ribosomal genes [33]. Canonical correlation analysis was used to integrate data from different batches by running the following steps as implemented in the Seurat package [34]: selection of integration features; removal of immunoglobulin genes from the features used for integration; preparation for integration with the PrepSCTIntegration function. Data integration was then performed using the FindIntegrationAnchors and IntegrateData functions based on the first 30 correlation components. PCA analysis was performed on the integrated dataset, and the first 12 principal components were used for UMAP computation and clustering (using 30 nearest neighbors and a resolution of 0.2). Cluster 1 was subclustered by executing the same steps described previously (PCA analysis on the subset and clustering computation with the first 10 principal components, 15 nearest neighbors, and a resolution of 0.2). The log-normalized expression values, marker genes for each cluster, as well as differentially expressed genes between conditions were inferred by the Wilcoxon test as implemented in the FindAllMarkers function. Cell cycle score and classification were calculated by CellCycleScoring function based on the expression of G2/M and S phase markers [35].

2.9. Study of BCL2 Promoter Mutations

For this study, DNA was phenol/chloroform extracted from:

1. The various cell lines listed in Section 1 (DoHH2, SU-DHL-4, SU-DHL-6, and OCI-Ly3) were used as positive controls for BCL2 promoter mutations;
2. Total spleen from iteratively immunized mice (4 $Ig\kappa$ -BCL2 /+ and 4 $3'$ RR-BCL2);
3. Class-switched versus non-class-switched B cells from additional groups of 3-month-old immunized $Ig\kappa$ -BCL2 /+ (3 mice) and $3'$ RR-BCL2 mice (3 mice). These mice were induced only once with SRBC and sacrificed on day 7. Single-cell suspensions from the spleen were stained with BV510 anti-CD19 (BD Biosciences, Clone: 1D3) and FITC anti-IgM (Southern Biotech, Cat number: 1020-02) antibodies. Cells were then sorted using the BD Aria III cell sorter to obtain class-switched B cells ($CD19^+$ /IgM $^-$) and non-class-switched B cells ($CD19^+$ /IgM $^+$);
4. From mice tumors:
 - Tumoral tissues of 3 $Ig\kappa$ -BCL2/+ mice;
 - Mesenteric LNs of one $Ig\kappa$ -BCL2/+ and one $3'$ RR-BCL2 tumoral mice;
 - Total spleen of two $3'$ RR-BCL2 tumoral mice.

The full promoter region of *BCL2* was then amplified by polymerase chain reaction (PCR) using specific forward (5' TGAATGAACCGTGTGACGTTACGC 3') and reverse (5' CTCAGCCCAGACTCACATCA 3') primers. The amplification of the PCR product (2,184 bp long) was verified by gel electrophoresis using agarose 2% gel in TBE. The amplified PCR product was then purified using the Nucleospin Gel and PCR Clean-up kit (Macherey-Nagel, Reference: 740609.250).

Next-generation sequencing was performed from amplified products (1 µg) according to the user guide of the Ion Xpress Plus gDNA Fragment Library Preparation (Life Technologies catalog no. 4471269), and libraries were sequenced on an Ion Proton System.

Two non-lymphoid controls were used for each library run, consisting of genomic tail DNA samples from an Igκ-*BCL2*/+ and a 3'RR-*BCL2* mouse, respectively. Analysis was performed using Deminer software developed by our laboratory in order to subtract the background level of mutations observed on the same sequence in a control experiment [36].

3. Results

3.1. Generation of Mice Carrying B-Cell Specific *BCL2* Deregulation

Hemizygous mice corresponding to our two *BCL2* deregulation models were studied. Both produced high amounts of a human *BCL2* protein of normal size in a B-lineage-specific manner (Figure 1A–D). Both revealed overexpression of human *BCL2* in spleen follicular and GC B cells, with a stronger expression in the Igκ-*BCL2* than in the 3'RR-*BCL2* mice (Figure 1D). In addition, *BCL2* expression patterns along B-cell differentiation stages strongly differed between the two models (Figure 1D). The Igκ-locus driven deregulation consisted of very high and stable *BCL2* overexpression throughout B-cell differentiation in the BM from B-cell progenitors to recirculating mature B cells, plasmablasts having migrated to the BM and mature plasma cells. This “knock-in” strategy also yielded a constitutively high expression in peripheral spleen and lymph node lymphoid tissues, homogeneously affecting all B-cell compartments but strongly culminating in plasmablasts.

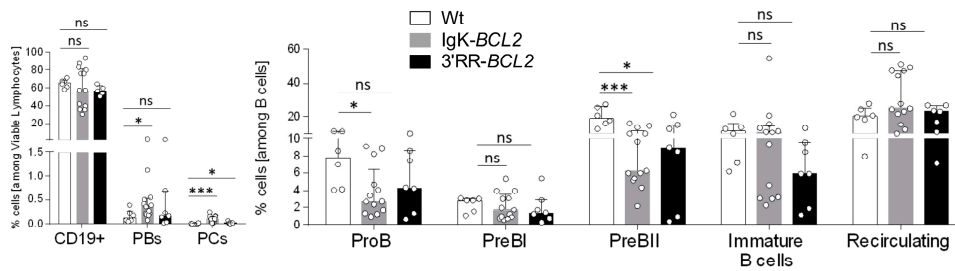
In striking contrast, the IgH 3'RR-*BCL2* drove low *BCL2* expression in BM B cell progenitors and plasma cells. In the spleen and lymph nodes, it provided the highest expression in GC B cells, either centrocytes or centroblasts, with expression remaining high without peaking in plasmablasts and falling down in plasma cells.

3.2. Impact of *BCL2* Deregulation on B- and T-Cell Differentiation

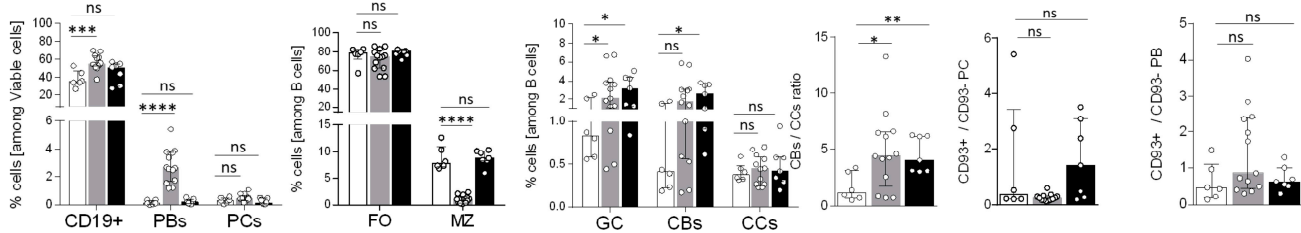
We analyzed B cell compartments by flow cytometry in non-immunized mice bred in a SOPF facility, comparing mutant mice to WT controls. Prior to any immunization, the percentage of BM CD19+ cells was similar in *BCL2*-deregulated models to that in WT controls and showed no amplification of any progenitor compartment, even with lower percentages of pro-B and pre-B cells in Igκ-*BCL2* mice (Figure 2A). In contrast, BM plasmablasts and PCs were constitutively increased in the Igκ-*BCL2* mice.

In the periphery of resting unimmunized mice, CD19+ cells were more abundant in Igκ-*BCL2* than in WT mice in both lymph nodes and spleen, while 3'RR-*BCL2* mice inconstantly showed such an increase. The difference between both strains was still more striking for plasmablasts and plasma cells, the amount of which was normal in 3'RR-*BCL2* mice but increased by up to ten-fold in Igκ-*BCL2* (Figure 2B,C). In contrast, marginal zone (MZ) cells were decreased in Igκ-*BCL2* mice. The ratio of CD93+CD138+ vs. CD93-CD138+ plasmablasts was rather increased in both strains, significantly in lymph nodes, suggesting an increased amount of recently differentiating plasmablasts [37]. In plasma cells, for which CD93 expression marks long-lived plasma cells (LLPCs) arising from T-dependent responses, there was a tendency to an increased ratio of such cells in the 3'RR-*BCL2* mice, but not reaching significance [37].

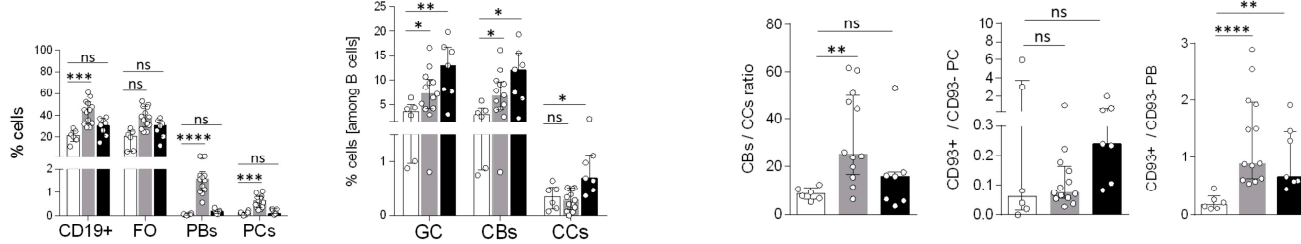
A. B-lineage cells in un-immunized mice (bone marrow)



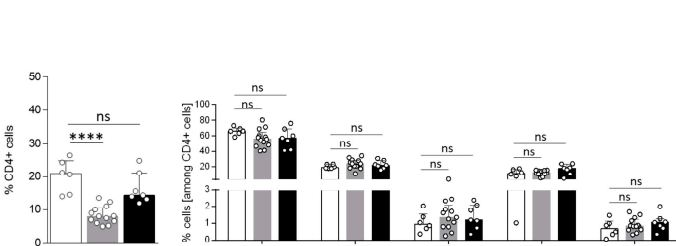
B. B-lineage cells in un-immunized mice (spleen)



C. B-lineage cells in un-immunized mice (mesenteric lymph nodes)



D. Peripheral T-cells (spleen)



E. Peripheral T-cells (mesenteric lymph nodes)

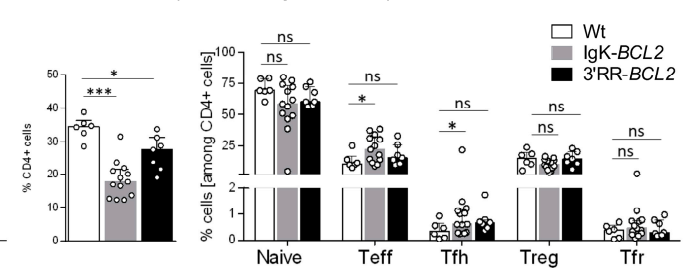


Figure 2. B cell development and lymphoid compartments in resting mice Flow cytometry data showing the impact of BCL2 deregulation alone, in both mouse models compared to WT mice in non-immunized conditions, on the different B cell compartments, in bone marrow (A), spleen (B) and mesenteric lymph nodes (C), as well as on the T cell compartment in spleen (D) and mesenteric lymph nodes (E). Percentages of the different cell compartments are presented as medians with interquartile range and the statistical significance was determined by the Mann–Whitney U test. Ratios for the centroblasts to centrocytes, as well as CD93+ to CD93– plasma cell (CD138+ CD19–) and plasmablastic cell (CD138+ CD19+) populations, are also presented (* $p < 0.05$; ** $p < 0.01$; *** $p < 0.001$; **** $p < 0.0001$). The full staining panel of both B and T cells is summarized in Supplementary Table S1.

Regarding the GC B-cell compartments in the spleen and mesenteric lymph nodes (corresponding to background GCs developed in non-immunized mice), both strains showed a constitutive increase in both centroblasts and centrocytes and an increased ratio of centroblasts vs. centrocytes.

Relative to expanded B-cell populations, the percentage of helper T cells appeared significantly decreased in the periphery of $Ig\kappa$ -*BCL2* mice only (Figure 2D), with a tendency for both *BCL2* strains to have less naïve T cells but slightly increased effector (Teff) and follicular helper T (Tfh) cell populations, only reaching statistical significance in the mesenteric LNs of the $Ig\kappa$ -*BCL2* mice (Figure 2E).

3.3. Lymphoid Compartments and Response to Immunization in *BCL2* Mice

Human lymphoid malignancies are often correlated with past chronic activation by viral Ag or auto-Ag, and we thus explored the behavior of *BCL2* transgenic mice in conditions of three consecutive B-cell stimulations with the particulate Ag SRBCs.

Such a repeated stimulation resulted in a strong global B-cell increase in all lymphoid tissues from $Ig\kappa$ -*BCL2* mice but not 3'RR-*BCL2* mice (Figure 3). The $Ig\kappa$ -*BCL2* also confirmed an MZ B-cell decrease.

In BM (Figure 3A), the B-cell increase corresponded to recirculating B-cells, whereas all B-cell progenitor compartments appeared to be decreased. Percentages and the absolute number of BM plasmablasts and plasma cells were also significantly increased in $Ig\kappa$ -*BCL2* mice.

In spleen and lymph nodes from $Ig\kappa$ -*BCL2* mice (Figure 3B,C), the global increase in CD19+ B cells was also associated with a strong increase in plasmablasts and to a lower extent of plasma cells. Plasma cells quantified after immunization did not show the above-mentioned increased ratio of CD93+ cells and did not yet express the markers of LLPCs. In contrast, a strongly increased ratio of CD93+CD138+ plasmablasts was seen in the spleen of $Ig\kappa$ -*BCL2* mice, indicating a high influx of recently differentiated cells [37].

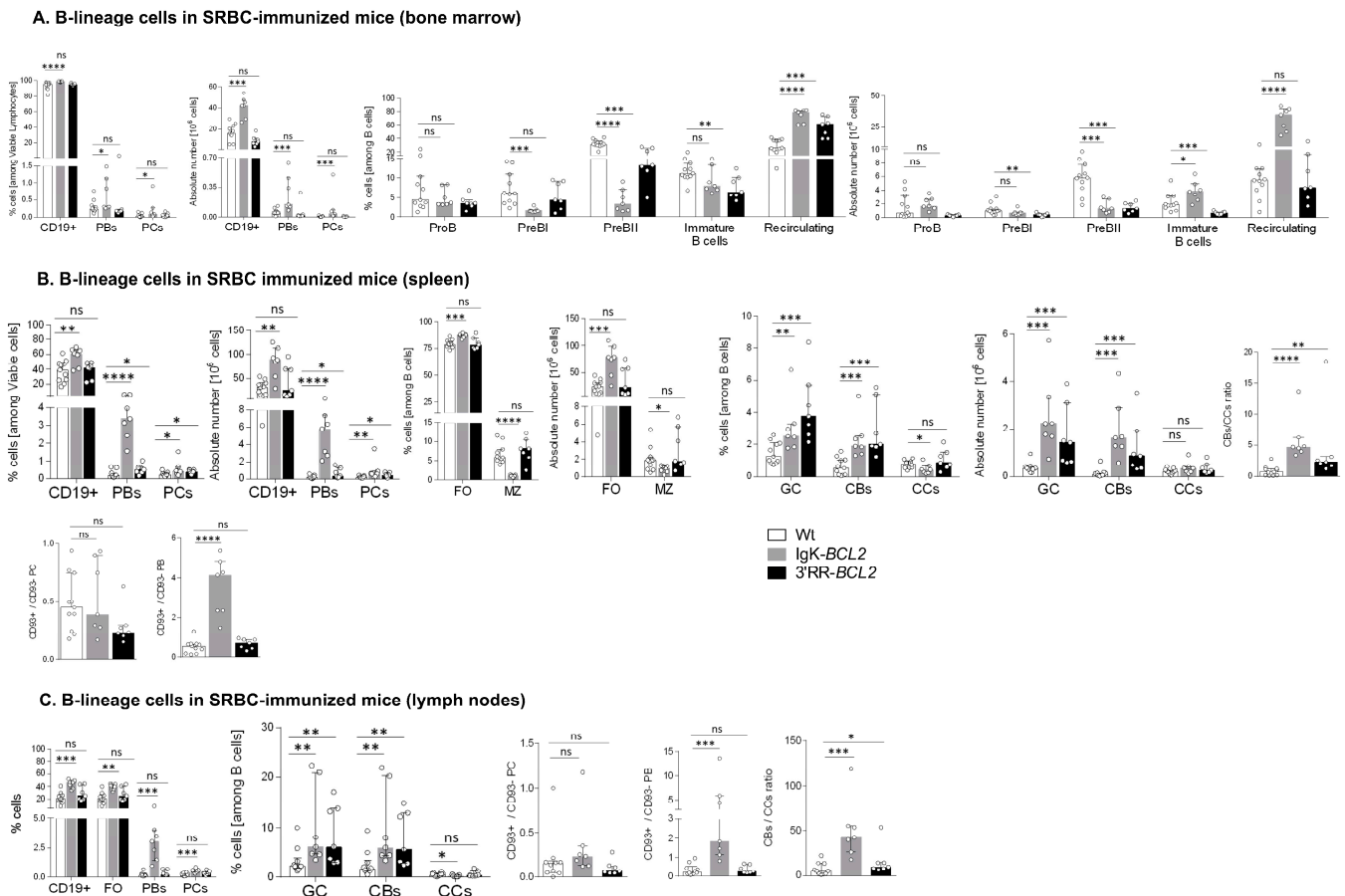


Figure 3. Cont.

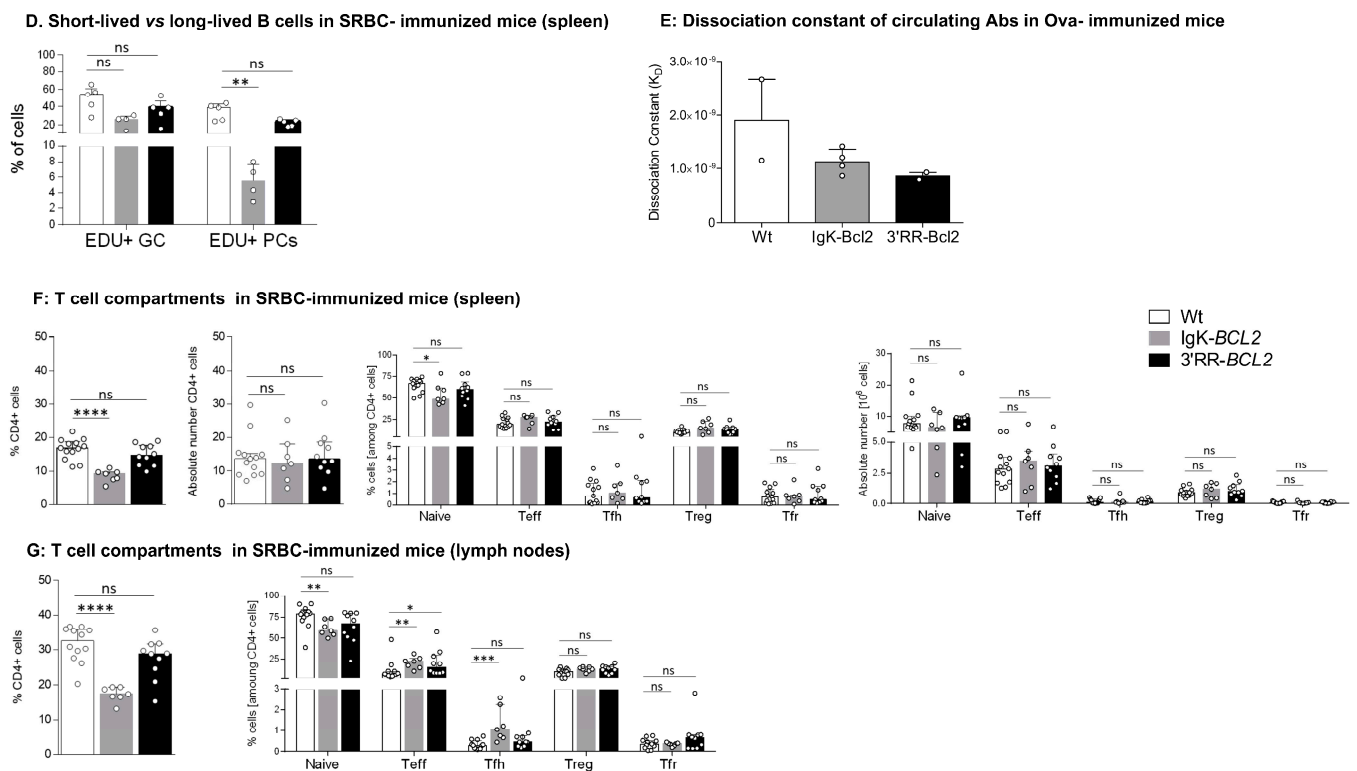


Figure 3. Immune responses in immunized mice (A–C) Impact of BCL2 deregulation on the immune response of immunized mice lymphoid tissues (bone marrow, spleen, and mesenteric lymph nodes, respectively), of intra-peritoneal immunization (3 iterative SRBC injections, on a monthly basis). B cells were evaluated by flow cytometry in BCL2 mice compared to WT. The ratios of centroblasts to centrocytes, as well as CD93+ / CD93- plasma cells and plasmablasts, are indicated. Percentages of the different populations, as well as absolute cell numbers (calculated based on the percentages obtained by flow cytometry and the total amount of lymphocytes in each organ), are presented as medians with interquartile range: statistical significance was determined using the Mann–Whitney U test. The full staining panel and gating strategy are summarized in Supplementary Table S1 and Supplementary Figure S1A–S1C. (D) Flow cytometry analysis of splenocytes stained with EDU (24 h post intraperitoneal EDU injection and 7 days after SRBC immunization) in WT (5), Igκ-BCL2 Δ/+ (4) and 3'RR-BCL2 mice (5). The percentages of EDU-stained plasma cells (EDU+ PC) and GC B cells (EDU+ GC) are medians with interquartile range. Statistical significance was determined using Mann–Whitney U test. EDU staining was revealed by coupling to Alexa 488, together with specific markers for plasma cells (CD138 BV786), GC B cells (GL7-APC and CD38-APC-R700), and cell viability (FVS 780). (E) Affinity of anti-Ova antibodies. Histogram of the dissociation constant (KD) of IgG to Ova, evaluated by ELISA, in the sera of BCL2 mice compared to WT. Lower KD marks a higher affinity for Ova. KD values are medians with interquartile range. (F,G) Flow cytometry data showing the impact of the BCL2 deregulation accompanied with 3 iterative intra-peritoneal SRBC injections (on a monthly basis) on the different T cell populations, in both BCL2 mouse models compared to WT, in the periphery (spleen and LNs). Both percentages and absolute cell numbers of each T cell population are presented as medians with interquartile range, and the statistical significance is realized via the Mann–Whitney U test. (* $p < 0.05$; ** $p < 0.01$; *** $p < 0.001$; **** $p < 0.0001$).

Compared to Igκ-BCL2 mice, 3'RR-BCL2 mice showed a more specific relative increase in GC B-cells, involving both centrocytes and centroblasts, together with a higher ratio of centroblasts vs. centrocytes, suggesting that BCL2 expression in these mice mostly impacted B-cell survival at the centroblastic stage.

In order to evaluate whether the GC increase in both models and the plasmacytosis in Igκ-BCL2 mice rather involved the ongoing entry of B-cells into the GC and plasma cell

stages or the accumulation of long-lived cells, we measured BrDU incorporation into GC B-cells and GC plasma cells one week after immunization (Figure 3D). Evaluation of BrDU incorporation in GC B cells showed a preserved ratio of recently divided vs. lately divided cells. In parallel, this experiment revealed a decreased ratio of BrDU+ / BrDU- plasma cells, indicating that in addition to the increased influx of plasmablastic cells, the accumulation of LLPCs also clearly contributed to peripheral plasmacytosis.

In order to further appreciate the functional impact of BCL2 expression on the ability of mice to mount an efficient immune response in the context of an altered GC regulation, we carried out immunization with the T-dependent antigen ovalbumin. We then quantified the affinity of anti-Ova IgG antibodies using an ELISA-based protocol for the calculation of the dissociation constant K_D (the higher the affinity of the produced antibody, the lower the K_D). This protocol showed that both BCL2 models were able to produce a large amount of high affinity circulating IgG with a K_D similar to that obtained in WT controls (or even with a tendency towards a lower value, i.e., higher affinity) (Figure 3E). This finding is reminiscent of observations previously performed for E μ -BCL2 mice, in which the selection of Ag-specific B-cells appeared to be maintained [38].

The relative representation of the various T-cell compartments after repetitive immune challenges with SRBC remained similar to those in resting mice, with a significant decrease in the peripheral helper T cell population in the Ig κ -BCL2 mice, together with increased T_H17 and T_H22 cell populations in the LNs of Ig κ -BCL2 mice (and to a lesser extent in 3'RR-BCL2 mice) (Figure 3F,G).

3.4. Early Impact of B-Cell Anomalies on Global Transcriptional Profiles from Lymphoid Tissue Populations

Beyond the abovementioned changes in B and T-cell populations shown by cell cytometry, we wished to evaluate the global impact of the B-lineage anomalies on lymphoid tissues. RNAseq evaluation of global transcriptomic profiles was thus carried out on a set of spleen and mesenteric lymph node samples (from the cohorts of mice iteratively immunized with SRBCs). Comparison of the cohorts of each type of BCL2-deregulated mice with WT controls showed significant changes in several typical signatures (Figure 4). Few differences were detected between WT and 3'RR-BCL2 mRNA profiles, except for enrichment for a GC signature in the latter. This signature involved genes for multiple well-known markers of GC B cells, including the transcription factors *Mef2b* and *Mybl1*; genes encoding GC-specific enzymes such as *Aicda* (the activation-induced deaminase gene) and *Hpse* (Heparanase); and genes encoding signaling proteins known as up-regulated in the GC, such as *Nugggc* (encoding the Slip-GC nuclear GTPase), *Rassf6*, *Rgs13*, and finally *Efnb1* (encoding the membrane protein Ephrin-B1) [39–42]. The global transcriptional analysis of whole lymphoid tissues, in contrast, showed no increase in the plasma cell signature in 3'RR-BCL2 samples.

A strong GC signature was also noticeable in Ig κ -BCL2 samples, especially in lymph nodes. However, in contrast to 3'RR-BCL2 samples, Ig κ -BCL2 samples differed from WT for several additional signatures (Figure 4). The more prominent one was a strong plasma cell signature including constant Ig heavy and light chain genes but also *Jchain*, *Sdc1* (*Syndecan 1*), *Bhlha15* (*Mist1*), and *Tnfrsf17* (*BCMA*), which are all classical markers of plasmablasts and plasma cells [43–45]. Additional changes notably consisted of significantly down-regulated genes and thus did not correspond to signatures expressed by expanded B-cells but rather reflected a global impact of the B-cell and plasma cell expansion on other cells from the lymphoid tissue microenvironment. This included the down-regulation of many genes involved notably in TGF β responses, but also in the inhibition of MAPK-dependent and of growth-factor-dependent responses. In addition, many myeloid-lineage specific genes, including *Klf6*, *CD83*, *Tagap*, *Fosl2*, and *Id2*, showed a clear down-regulation in Ig κ -BCL2 samples, while a few of them were up-regulated (such as *Bst2* and *Siglec-H*, two genes notably expressed in plasmacytoid dendritic cells) [46], altogether suggesting a change

in the polarization of myeloid cells in the microenvironment of lymphoid tissues with BCL2-deregulated B cells (Figure 4).

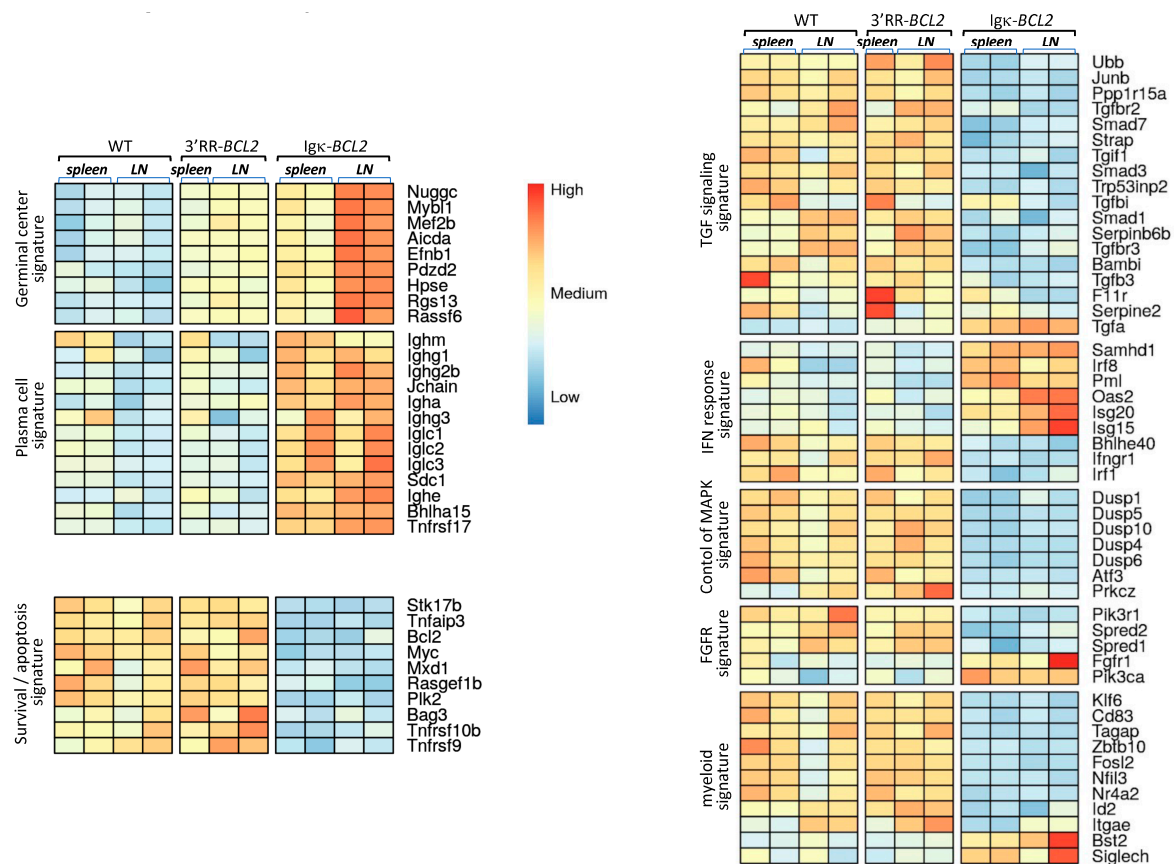


Figure 4. Transcriptomic signatures in whole lymphoid tissues from SRBC-immunized animals. Main transcriptional signatures, combining genes with significant variations, comparing WT to 3'RR-BCL2 and Igκ-BCL2 RNAseq profiles from lymphoid tissues (spleen and mesenteric lymph nodes) taken from SRBC-immunized mice.

3.5. Single-Cell Transcriptome Analysis

In order to appreciate the impact of BCL2 deregulation on the B-cell transcriptome more precisely than by global analysis of lymphoid tissues or by following a limited set of markers by cell cytometry, we carried out a single-cell analysis of purified B-lineage splenocytes 10 days after immunization by SRBCs. This analysis allowed identifying 12 clusters and sub-clusters. The top differentially expressed genes are indicated in Supplementary Figure S2. From their transcriptional profiles, clusters were identified as transitional cells, recirculating resting B-cells, extrafollicular and interfollicular cells, IFN-activated cells, marginal zone, pre-centroblastic, centroblasts, early centrocytes (*Aid*⁺ *Bcl6*⁺), late centrocytes (*Aid*⁻ *Bcl6*⁺), preplasmablasts, plasmablasts, and plasma cells (Figure 5A). This analysis confirmed and extended the observations made by flow cytometry. In particular, all compartments upstream of GC formation were rather decreased in BCL2 transgenics (from transitional cells to resting, extrafollicular, IFN-activated, marginal zone, and pre-centroblastic cells). In the Igκ-BCL2 model, the amplified compartments began with centrocytes but then culminated with plasmablasts and plasma cells. In contrast, in the 3'RR-BCL2 model, the amplified subclusters were more “GC-focused”, including centroblasts, centrocytes, late centrocytes, and plasmablasts (Figure 5B). This analysis also allowed for monitoring the mean expression level of a number of highly expressed genes comparatively between WT, Igκ-BCL2, and 3'RR-BCL2 mice. With more precision than in flow cytometric measurements, it showed a broad overexpression of BCL2 in all subclusters

in the $Ig\kappa$ -*BCL2* model, compared with a lower and much more specific expression in $3'$ RR-*BCL2* B cells, focused on centroblasts, centrocytes, and plasma cells (Figure 5C).

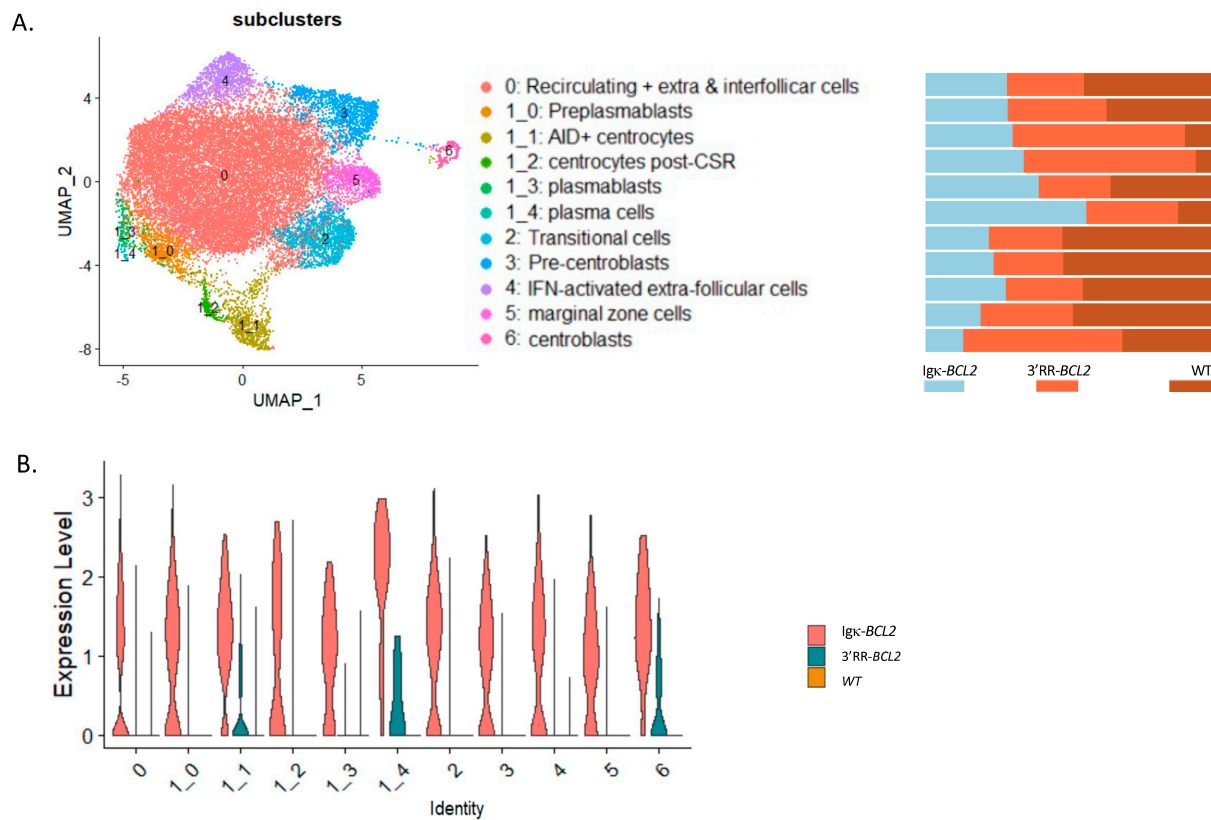


Figure 5. Single-cell RNAseq analysis of splenocytes from immunized mice: (A, left panel) UMAP of the $10\times$ single cell analysis of spleen B-cells 10 days after SRBC immunization, split into 12 clusters (as defined in Supplementary Figure S2). (A, right panel) Quantitative variations in cell numbers in the various clusters in $Ig\kappa$ -*BCL2* and $3'$ RR-*BCL2* mice compared to WT. (B) Human *BCL2* expression level in the various cell clusters in $Ig\kappa$ -*BCL2* and $3'$ RR-*BCL2*.

3.6. B-Cell Diversity in Young Immunized Mice

Ig repertoires of 3-month-old immunized mice only showed minor changes in comparison to normal mice (Figure 6), without a significant increase in the Gini index in any of the Ig transcript categories analyzed (μ or γ IgH transcripts from spleen or lymph nodes), thus indicating at this stage that no clonal amplification was detectable but that normally diversified repertoires were expressed after immunization. The usage of VH subgroups associated with IgH μ or γ transcripts showed no significant variation compared to WT mice.

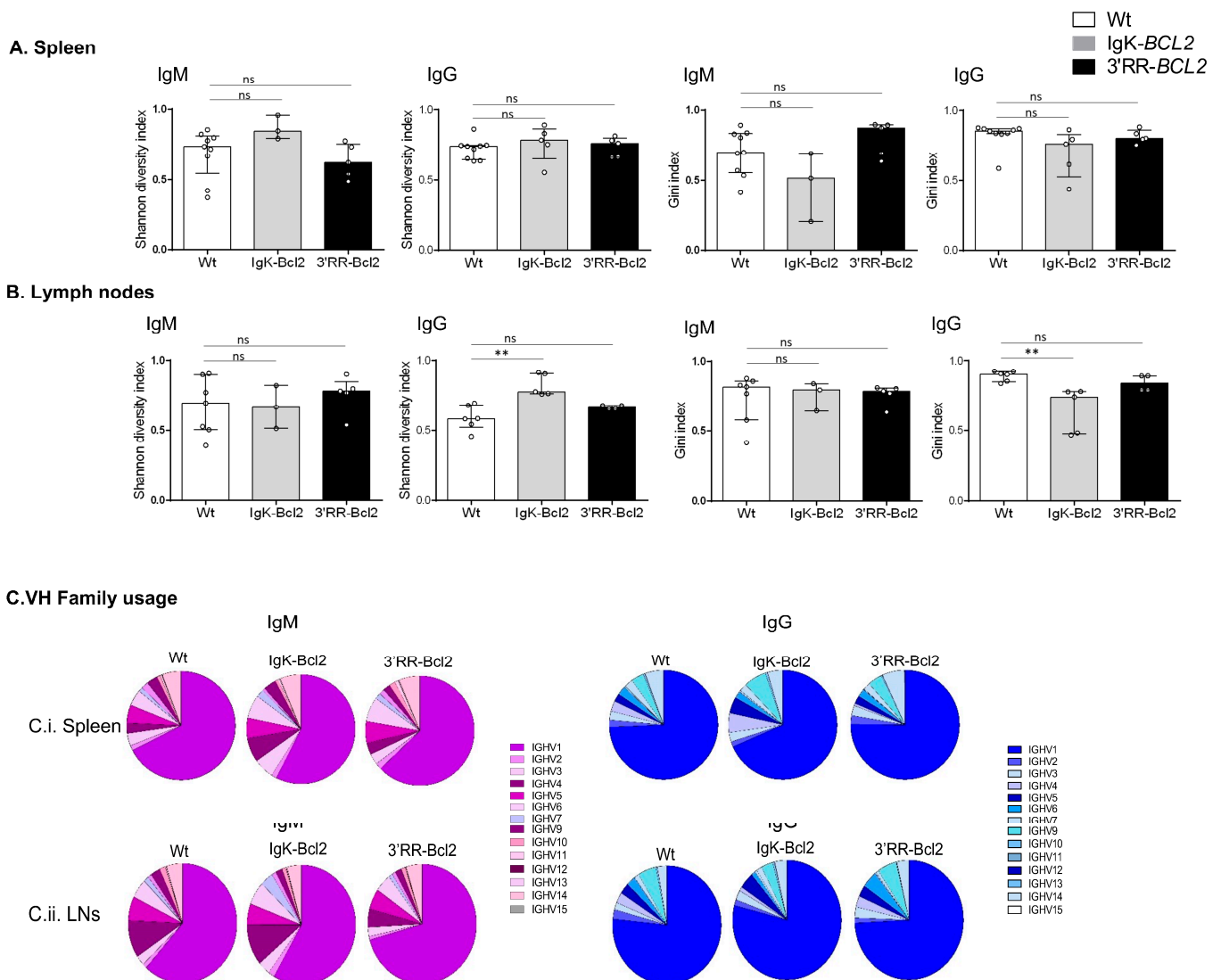


Figure 6. IgH repertoire of immunized mice. Histograms showing the Shannon diversity index and the Gini index of both IgM and IgG repertoires in the spleen (A) and mesenteric LNs (B) of both BCL2 mouse models compared to WT. Both indices are presented as medians with interquartile range, and statistical significances are determined by Mann–Whitney U test. (C) Pie charts showing the mean percentage of each VH gene family usage of both IgM (in purple) and IgG (in blue) in the spleen and mesenteric LNs of both BCL2 mouse models compared to WT. ** $p < 0.01$; ns, not significant.

3.7. Immunohistochemical Analysis and Tumor Development in BCL2 Transgenic Mice

We allowed cohorts of 40 mice for each genotype to grow older in order to monitor the potential onset of spontaneous tumors. Aggressive tumors indeed started to appear at ages 41 to 117 weeks in 10 homozygous Ig κ -BCL2/Ig κ -BCL2, 9 heterozygous Ig κ -BCL2/+ mice, and 6 3'RR-BCL2 mice (Table 1 and Figure 7A).

Table 1. Description of tumors: Table describing the mice that developed tumors in both BCL2 models. This cohort comprised 19 Igκ-BCL2 (total), and 8 3'RR-BCL2 mice were allowed to grow older, and these tumors were monitored for tumor development over time. For each mouse, the age at which they developed the tumor (or pre-tumoral symptoms), along with a detailed description of the location and the phenotype of each tumor, is listed.

| Genotype | Number | Age (weeks) | Ascitis | Tumor | Organs Affected / Tumor Description | Other Observations |
|-----------------|--------|-------------|---------|-------|--|----------------------------------|
| Igκ-Bcl2 Δ/Δ | KI-1 | 85 | ✓ | ✓ | Intestine, Mesenteric LNs, Cervical LNs, Splenomegaly (165 mg) | / |
| | KI-2 | 50 | X | ✓ | Intestine, Mesenteric LNs, Cervical LNs, Splenomegaly (650 mg) | / |
| | KI-3 | 71 | ✓ | ✓ | Intestine, Stomach, Splenomegaly (395 mg) | / |
| | KI-4 | 90 | X | ✓ | Intestine, LNs | occlusion |
| | KI-5 | 71 | X | ✓ | Mesenteric LNs, Liver, Splenomegaly (1580 mg) | / |
| | KI-6 | 54 | ✓ | ✓ | Stomach, Intestine, Mesenteric LNs, Liver, Pancreas, Splenomegaly (305 mg) | / |
| | KI-7 | 54 | ✓ | ✓ | Kidneys, LN atrophy, Splenomegaly (950 mg) | / |
| | KI-8 | 105 | X | ✓ | Mesentery, Liver, Kidneys, Splenomegaly | / |
| | KI-9 | 109 | ✓ | ✓ | Liver, Splenomegaly (397 mg) | / |
| | KI-10 | 70 | X | ✓ | Stomach, Liver, Splenomegaly (287 mg) | / |
| KI BCL2 Δ/+ | KI-11 | 92 | ✓ | ✓ | Under lungs, Mesenteric LNs, Splenomegaly (145 mg) | Diffused and bloody cervical LNs |
| | KI-12 | 84 | X | ✓ | Splenomegaly, Liver, Kidneys | Swollen testicles |
| | KI-13 | 117 | ✓ | ✓ | Intestine, Atrophy of all LNs, Splenomegaly (2500 mg) | / |
| | KI-14 | 52 | X | ✓ | Atrophy of cervical LNs, Splenomegaly (300 mg) | Obese |
| | KI-15 | 52 | X | ✓ | Splenomegaly (300 mg) | Obese |
| | KI-16 | 41 | X | ✓ | Mesentery, Splenomegaly | / |
| | KI-17 | 81 | X | ✓ | Mesentery, Splenomegaly | / |
| | KI-18 | 111 | X | ✓ | Mesentery, Splenomegaly | / |
| | KI-19 | 79 | ✓ | ✓ | Mesentery, splenomegaly (1350 mg) | Decolored liver |
| 3'RR-Bcl2+ | Tg-1 | 74 | X | ✓ | Atrophy of inguinal and axillary LNs, Splenomegaly (380) | / |
| | Tg-2 | 74 | X | ✓ | Splenomegaly (161 mg) | / |
| | Tg-3 | 60 | X | ✓ | Splenomegaly (240 mg) | / |
| | Tg-4 | 60 | X | ✓ | Splenomegaly (222 mg) | / |
| | Tg-5 | 64 | X | ✓ | Atrophy of cervical LNs Splenomegaly (222 mg) | / |
| | Tg-6 | 64 | ✓ | ✓ | Intestine, Liver, Atrophy of cervical LNs, Splenomegaly (730 mg) | / |
| | Tg-7 | 121 | X | ✓ | Mesentery, Splenomegaly (1139 mg) | / |

Representative immunohistochemistry analyses of tissues either from young mice (in the pre-malignant stage) or old mice with overt tumor development (notably 3'RR-BCL2 mouse Tg-6 and Igκ-BCL2/Igκ-BCL2 mouse KI-8 in Table 1) are shown in Figure 7B.

At the pre-malignant stage, the spleen showed a broadly normal architecture but with large follicles densely occupied with CD19+ B cells mixed with less abundant plasma cells. In such young 3'RR-BCL2 mice, BCL2 staining mostly marked B cells within GCs. On the contrary, in the Igκ-BCL2 mice, abundant plasma cells already populated the red pulp at the early stage and stained strongly for BCL2.

Later, in mice carrying overt tumors from either genotype, the spleen red pulp appeared heavily infiltrated by CD138+ BCL2+ plasma cells. These tumors affected mostly the mesenteric lymph nodes, spleen, and liver. The tumors analyzed at other distant locations also consisted of CD138+ cells, and the disease thus appeared similar to a disseminated plasmablastic lymphoma (Figure 7B).

Ig repertoire analysis by REPseq was performed for tumors from four Igκ-BCL2/Igκ-BCL2 tumoral mice (KI-2, KI-3, KI-4 and KI-8), three Igκ-BCL2/+ tumoral mice (KI-16, KI-18, and KI-19), and one 3'RR-BCL2 tumoral mouse (Tg-6) (Table 2). All tumors analyzed in both strains included one or eventually two strongly predominant clonal cell populations, each so-called "predominant clonotype" representing 30% to 98% of all Ig reads (Table 2). In only two cases, the VDJ region included an N-glycosylation site, which was germinally encoded. Both IgM-producing and IgG clones were found, with five of them carrying no mutation of the expressed VDJ region, while seven showed some level of somatic hypermutation (from 1 to 21 mutations/Kbp), indicating that malignant clones could originate in some cases from an extra-follicular pathway or in other cases be GC-derived.

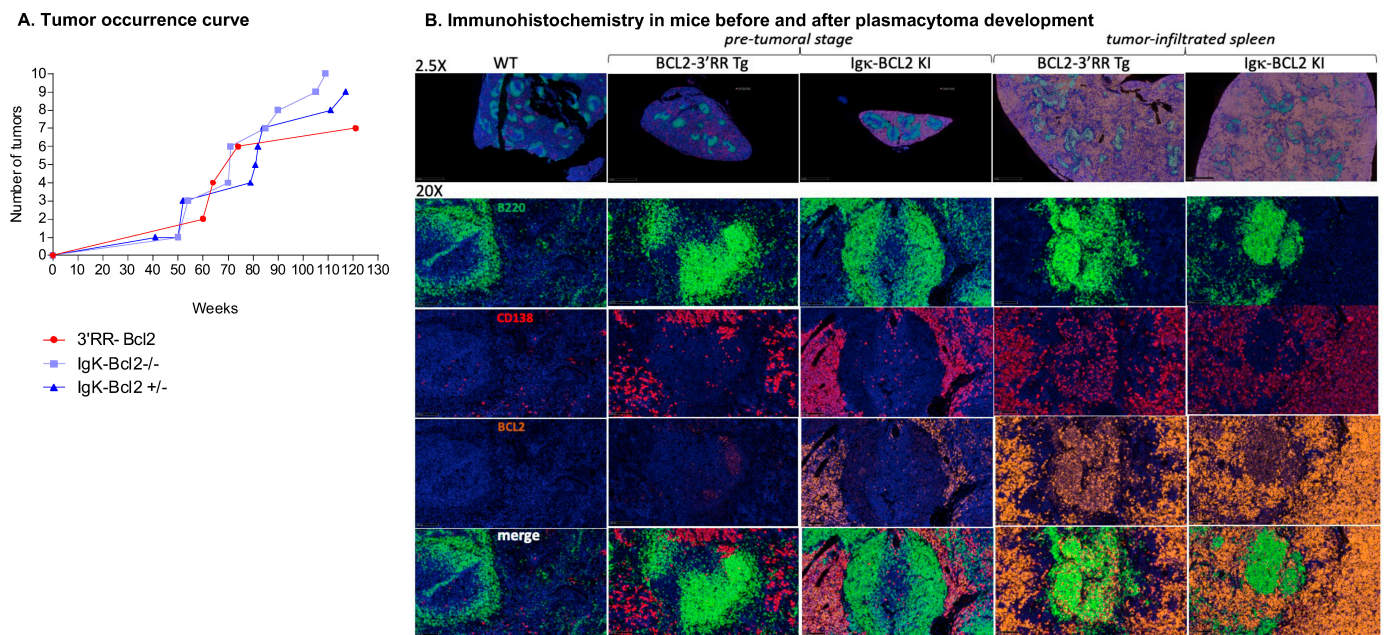


Figure 7. Tumors in BCL2 mice: (A) Curve showing the evolution of tumor occurrence in both BCL2 models with respect to their age (in weeks). (B) Immunohistochemistry (IHC) analysis of the spleen at the pre-tumoral and tumor-infiltrated stage of both BCL2 models compared to WT. Staining was performed for B cells (using B220 in FITC \cap Green), plasma cells (CD138 in TRITC \cap Red), human BCL2 (in cyanine 5 \cap Yellow), and finally, DAPI in blue.

Table 2. Mutation in the expressed V region of mouse tumor samples. Table showing the detailed IgM and IgG repertoire analyses of the tumor tissues of mice from both BCL2 models. Total number of clones for each heavy chain and the corresponding number of productive reads are indicated. Based on the previous repertoire data obtained from WT mice, a certain threshold for the clone frequency was used, and only the clones that were present at a frequency higher than or equal to 30% were selected. For each clone, the V and J genes used along with their corresponding V mutation frequency (without CDR3 as it is highly mutated) are also indicated.

| Genotype | Mouse nb | Heavy Chain | Total Number of Clonotypes | Total Number of Productive Reads | V_Gene | J_Gene | Clonotypic Predominance (Clones \geq 30%) | V_Mutation Frequency (without CDR3) per kb |
|--------------------------|----------|-------------|----------------------------|----------------------------------|----------|--------|---|--|
| IgK-BCL2 Δ/Δ | KI-2 | IgG | 234 | 1269 | IGHV4-1 | IGHJ2 | 42.2 | 1 |
| | KI-3 | IgM | 248 | 9087 | IGHV6-3 | IGHJ2 | 95.2 | 21 |
| | | IgG | 58 | 8308 | IGHV10-3 | IGHJ2 | 99 | 3.5 |
| | KI-4 | IgM | 430 | 2104 | IGHV4-1 | IGHJ2 | 47.6 | 0 |
| | | IgG | 1055 | 6274 | IGHV1-5 | IGHJ3 | 30.2 | 15 |
| | KI-8 | IgM | 143 | 1560 | IGHV3-6 | IGHJ2 | 64.4 | 18 |
| IgG | | 26 | 2835 | IGHV4-1 | IGHJ2 | 98.4 | 8 | |
| IgK-BCL2 $\Delta/+$ | KI-16 | IgG | 15 | 871 | IGHV10-1 | IGHJ2 | 98.8 | 0 |
| | KI-18 | IgG | 74 | 175 | IGHV10-3 | IGHJ2 | 41.1 | 3.5 |
| | KI-19 | IgM | 494 | 2106 | IGHV1-39 | IGHJ2 | 53.4 | 0 |
| | | IgG | 619 | 11924 | IGHV1-26 | IGHJ2 | 85.2 | 0 |
| 3'RR-BCL2 | Tg-6 | IgG | 1157 | 12395 | IGHV2-2 | IGHJ4 | 51.1 | 0 |

Clones carrying a VDJ N-glycosylation site are in red.

3.8. The BCL2 Cassette Is Exposed to Low SHM in Both Transgenic Models

Sequencing the promoter region of BCL2 in both models revealed that SHM occurred all along a 1.5 kb sequence fragment and globally appeared diversified in polyclonal cells (in agreement with the B-cell diversity indicated by Ig repertoire experiments) in mice not affected with tumors (Figure 8). The mutation rate at a given position thus never exceeded 0.6%. Sequences with the highest rate of SHM were rather obtained in class-switched B

cells from immunized Igκ-BCL2 mice, and the most frequently mutated positions were located around the P1 promoter.

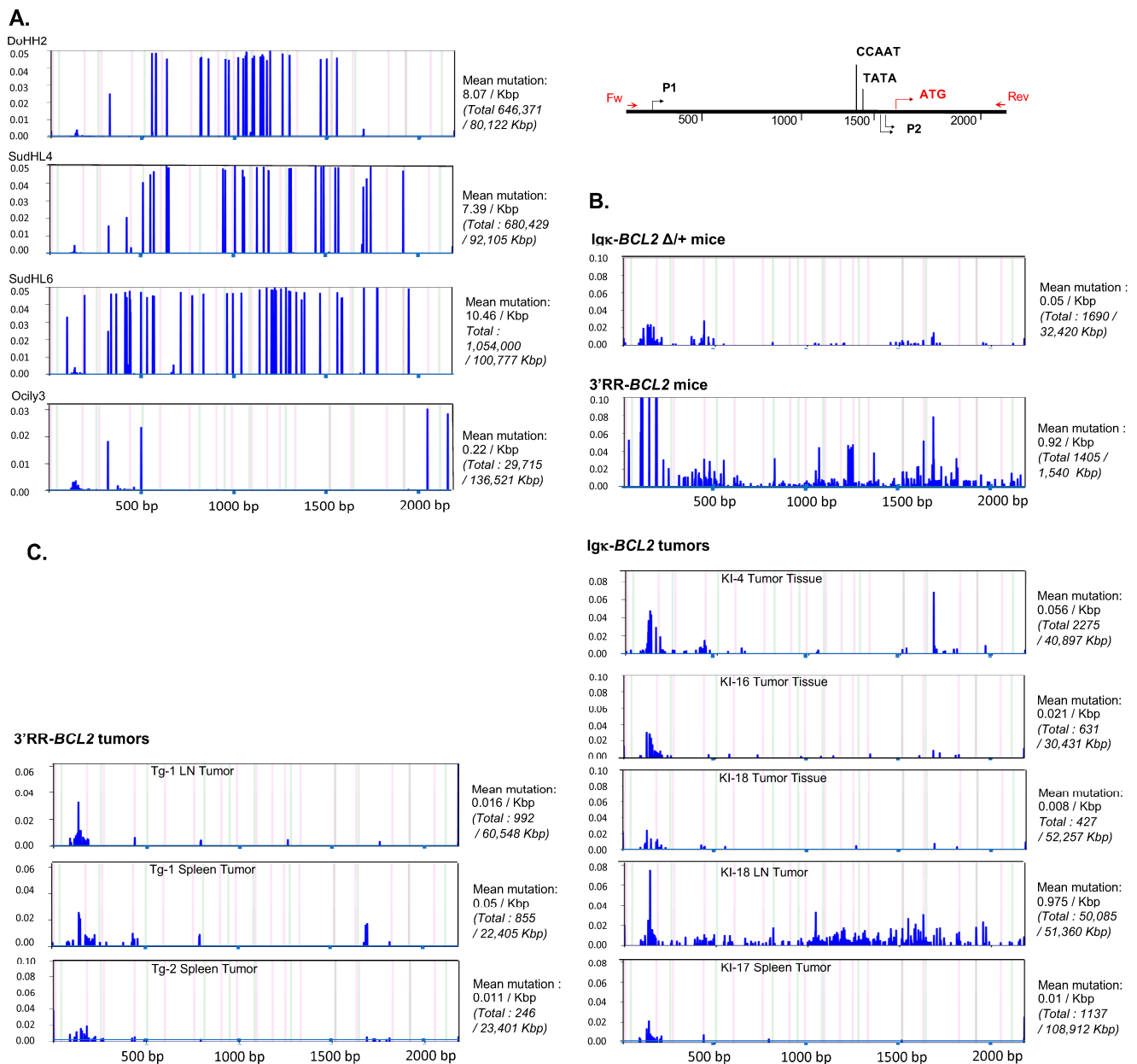


Figure 8. Mutation in the Bcl2 promoter region. Graphs showing the frequency and the localization/distribution of mutations along the BCL2 promoter region (after high-throughput sequencing) as well as the global mutation rate and the mutation enrichment in AID-hotspots in several human DLBCL cell lines as positive controls (A), in total splenocytes or class-switched versus non-class-switched splenocytes of immunized mice (3 iterative immunizations or single 7-day immunization, respectively) from both BCL2 models (B) and finally in various tissues/organs from several tumoral mice of both BCL2 models (C). Graphs are shown as generated by the system Deminer after correction with respect to two negative controls passed on the same run.

In some but not all tumors, mutations were present at a higher level, eventually approaching 10% of the reads.

4. Discussion

Deregulation of the *BCL2* oncogene is observed in multiple different types of B-cell malignancies, with diverse patterns of expression, and the translocation of the oncogene to the IgH locus is the classical hallmark of FL [1]. This translocation and other alterations of the *BCL2* locus architecture, such as either translocation to Ig light chain genes or chromosomal amplifications of the *BCL2* locus, are also documented either in some rare FL cases, in DLBCL or in chronic lymphocytic leukemia cases [3–5]. In addition to *MCL1*-dependence, about 20% of myeloma cases, and notably those featuring t(11;14) translocations, are co-dependent from *BCL2* deregulation and are thus responsive to *BCL2*-targeted therapy using venetoclax [47,48]. Altogether, diverse patterns of *BCL2* deregulation clearly impact the phenotype of *BCL2*-driven B-cell malignancies in patients.

Regarding mouse models, the most popular *BCL2* deregulation models are the E μ -*BCL2* transgenics, with broad *BCL2* deregulation at all B-cell stages, and the vavP-*BCL2* mice, with broad overexpression in both B and T cells [19,20,24]. We thus currently lack optimal mouse models for precisely reproducing the maturation stage-specific anomalies that support the development of human *BCL2*-driven B-cell malignancies.

We herein reported two new models of B-lineage-specific *BCL2* deregulation in mice. These models yield different patterns of expression, either with a restricted GC-specific expression in transgenics driven by the IgH 3'RR or with a global *BCL2* overexpression in the Ig κ -*BCL2* knock-in strain, which affects all mature B-cell stages, including GC cells and reaches a climax in plasma cells. Although both models roughly yield deregulated expression in GC B cells, the high “GC-specificity” of the 3'RR-driven model makes it a potentially attractive “first hit” platform for studying early events of FL lymphomagenesis. Indeed, FL is currently considered as evolving from FLLC cells carrying an initial t(14;18) translocation then, followed by multiple additional driver mutations, the latter concurring to block plasma cell differentiation and the exit of the transformed cells from the GC stage.

In contrast, the broad deregulation and highest expression of the oncogene in both GC B-cells and plasmablasts observed after the Ig κ -*BCL2* knock-in principally shows up with an early polyclonal expansion of the plasmablastic and plasma cell compartments in young mice, prior to any immunization. This plasmacytosis also involves both an increased influx of plasmablasts and the accumulation of long-lived plasma cells. In old animals, the pre-malignant plasmacytosis can then end with monoclonal or oligoclonal plasma cell tumors, and this mouse strain could thus provide a pertinent model for *BCL2*-driven plasma cell dyscrasia, which is notably a frequent feature of t(11;14) human myeloma cases [47,48].

Homeostasis of immune cells in lymphoid organs is strongly dependent upon inter-cellular interactions, and both lymphoid and plasma cell malignancies are known to strongly involve interactions between B-cells and their microenvironment in lymphoid tissues [16,49]. In this regard, it is interesting to notice that the altered B-cell homeostasis in such B-cell-specific *BCL2* deregulation models has an early impact on non-B cells from the lymphoid microenvironment long before the development of overt B-cell malignancy. Notably, the imbalance of B-lineage compartments significantly alters T-cell populations, with lower amounts of naïve T cells but higher amounts of effector T cells and Tfh cells in the 3'RR-*BCL2* model than in WT animals, suggesting a global GC expansion, not restricted to GC B-cells. In contrast, in the Ig κ -*BCL2* mice developing polyclonal plasmacytosis, transcriptional analysis of lymphoid tissues shows not only a strong and expected over-expression of a plasma cell signature but also the significantly decreased expression of multiple genes, with signatures related to TGF β signaling, IFN signaling, inhibition of MAPK signaling, and a strong down-regulation of many genes mostly specific for myeloid cells. It remains to be explored whether these early anomalies could pave the way for the future development of a suppressive tumoral microenvironment once aged mice develop plasma cell dyscrasias.

Finally, regarding the occurrence of spontaneous tumors, this preliminary characterization of mice solely affected with *BCL2* deregulation and no additional oncogenic hit

shows that only some aged animals developed tumors. All consisted of plasma cell tumors, whatever the genotype, and whether or not the tumor was preceded by overt polyclonal plasmacytosis as seen in the Ig κ -*BCL2* mice.

Mice from both genotypes were able to mount normal humoral responses, and the polyclonal expansion of some B-cell compartments was thus not associated with any differentiation blockade, which could have hampered the production of specific antibodies. A similar situation is likely occurring for human FLs only deregulating *BCL2*, which circulate and are reportedly identified in blood and lymphoid tissues from healthy individuals without any differentiation blockade [50,51]. In contrast, local amplification of a more aggressive B-cell clone, either in the early situation of in situ follicular neoplasia or of overt FL, is always associated with mutations additional to the *BCL2* deregulation [52]. The most obvious roles of all such additional mutations, notably involving chromatin modifier genes such as CREBBP, EZH2, or KMT2D, is to reprogram B-cells towards an iterative GC reentry cycle by up-regulating *BCL6* expression and inhibiting genes involved either into B-cell egress from the GC and/or into plasma cell differentiation and progress beyond the GC B-cell stage [53–56].

Although we have no indication about the eventual supplemental hits supporting the growth of plasmacytoma in aged *BCL2* mice from our current study, acquired genetic or epigenetic anomalies are likely since no tumor arises in young mice, whatever the *BCL2* expression dosage. In both mouse strains, B-cell repertoire diversity in young tumor-free animals appears normal, without monoclonal or oligoclonal pre-malignant expansion. Spontaneous and random genetic anomalies accounting for the development of plasma cell malignancies in older animals then clearly did not block plasma cell differentiation and/or egress from the GC. As for previously reported *BCL2* deregulation models, the development of lymphoma in such mice will thus need on-purpose breeding with mouse strains carrying the same types of second hits seen in human GC lymphomas [16,53–56].

Contrary to our expectations, the presence in those mouse models of a complete P1/P2 *BCL2* promoter fragment, including the negative regulatory sites for *BCL6* binding, does not repress *BCL2* expression in GC B-cells strongly express the mouse transcription factor *Bcl6*. This promoter is not affected either by obviously acquired mutations unleashing expression in some B-cell clones. Although the P1/P2 fragment is accessible to a significant amount of SHM, notably when inserted in the Ig κ locus, these mutations rather seem to accumulate randomly at a low level. The spontaneously high expression of *BCL2* in either model appears sufficiently high by itself for supporting the outgrowth of clonal malignant tumors without the need for promoter mutations.

Tumors occurring in both models are mostly made up of clonal plasma cells (with biclonal proliferations in some cases), either producing IgG or IgM with roughly similar frequencies and revealing SHM of VH genes ranging from 3.5 to 21 per Kbp for 7 out of 12 malignant clones, thus with a clear indication of a “post-GC” origin of the malignant clones. GC-derived plasma cells have indeed been described with a strongly higher SHM rate in comparison to extrafollicular plasma cells (mean 5.6 mutations/Kbp vs. 0.7/Kbp) [57]. In 5 out of 12 malignant clones studied, completely germline Ig sequences were expressed by the monoclonal B-cell clone, the origin of which was thus rather extra-follicular and independent of T-cell help.

Although attributed to V(D)J recombination errors, which could potentially affect any Ig locus, *BCL2* translocations associated with FL in patients overwhelmingly involve the IgH locus on chromosome 14 and much more rarely Ig light chain loci [3,58]. Such translocations replace all the IgH V gene clusters with *BCL2* and thus associate the oncogene with regulatory elements for the IgH constant gene cluster, hereby predominantly placing the oncogene under the control of the IgH 3'RR in mature B-cells. Such conditions yield strong *BCL2* expression in activated B-cells and at the GC stage undergoing 3'RR-dependent SHM and CSR, as reproduced in our 3'RR-*BCL2* mouse model.

That both *BCL2* strains from this study differ for the polyclonal plasma cell expansion developed in Ig κ -*BCL2* mice reveals an unexpected impact of the *BCL2* level on B-cell

homeostasis. The ability of B-cells to mount high-affinity Ag-dependent responses after immunization is, however, preserved in both *BCL2* models. Since the expansion of GC B-cells (in 3'RR-*BCL2* mice) and the expansion of GC and plasma cells (in Ig κ -*BCL2* mice) does not occur at the expense of other B cell compartments, they are unlikely to result from impacts on cell fate decisions, for example making Ig κ -*BCL2* cells more prone to engage into plasma cell rather than memory B-cell differentiation when BCL2 exceeds a certain threshold.

The simplest explanation for the observed expansion of some B-cell compartments is rather a lower level of cell death within GCs for both models, then increasing the influx of all GC and post-GC cells. Specifically in the Ig κ -*BCL2* model, the prolongation of BCL2 overexpression beyond the GC or extra-GC B-cell activation stages then additionally increases the half-life of cells transiting through the plasmablast stage and finally supports the accumulation of LLPCs. Initial steps of plasma cell differentiation are indeed known to depend on endogenous BCL2 expression [59], and survival thus initially increases when BCL2 expression fails to tamper in transgenic Ig κ -*BCL2* plasmablasts. Later on, LLPCs normally do not rely on BCL2 for their survival but rather on BCMA-dependent MCL1 expression [59]. Since MCL1 and BCL2 share a similar pro-survival function, maintaining or even increasing expression of the knock-in Ig κ -*BCL2* in all PCs necessarily ends with deregulated survival and hypertrophy of the LLPC compartment. Plasma cells are also strongly exposed to endothelial reticulum (ER)-mediated stress, which triggers autophagy and mitophagy. The higher Ig κ -*BCL2* expression might then reach a threshold for which non-classical functions of BCL2 can be heightened beyond its main role in mitochondrial outer membrane permeability. BCL2-family members such as BCL2-L13 and BNIP3 are indeed also major actors of autophagy and mitophagy [60,61]. These factors share interactions with some BCL2 partners, such as BECLIN-1, and their function in promoting mitophagy might likely be hampered by excessive amounts of BCL2. Noticeably, human myeloma often associates up-regulation of MCL1 and silencing of BNIP3 [62]. Altogether, either by reducing ER-stress-induced apoptosis, autophagy, or mitophagy, the BCL2 up-regulation triggered at the plasmablast/plasma cell stage in Ig κ -*BCL2* mice appears to open up the gate for entry of more B cells into the plasma cell stage together with deregulated accumulation of non-dying LLPCs. This model hereby appears as ideally suited for yielding a permanent polyclonal expansion of plasma cells and then provides an ideal platform for studying the second hits, which more profoundly affect homeostasis and support the development of plasma cell dyscrasias.

5. Conclusions

In comparison to the most widely used vavP-BCL2 model, the two models reported in this study are of high interest due to their complete B-cell specificity, while in contrast, vavP-BCL2 mice largely express BCL2 in other hematopoietic lineages and notably T-cells [24]. Interestingly, our study shows that even B-cell specific deregulation can indirectly affect the other cell populations present in lymphoid tissues, showing a B-cell impact on the lymphoid micro-environment even in pre-malignant conditions and then providing ideal conditions for studying the evolution of cell interactions along lymphomagenesis.

At this stage, our study of mice carrying a single on-purpose mutation obviously carries limitations. In contrast, spontaneous human lymphomas often combine multiple oncogenic anomalies [63]. We indeed compared two different locations of the same oncogenic cassette, but various parameters differ in these two architectures. Our main guess is that the IgH 3'RR is providing a higher specificity of expression for those stages corresponding to activated B-cells and GC B-cells and could thus provide optimal pre-malignant settings for lymphomas of the GC or post-GC type. It is indeed noticeable that the 3'RR not only includes transcriptional enhancers but also sites for transcriptional repression after binding factors such as Bach2, Mafk, and Pax5 [64–67]. In contrast, expression of a knock-in oncogene within the Igk locus yields expression at all B-cell stages under the influence of both the intronic Ek and the downstream kE3' enhancer. By analogy, the Igk

chain expression, BCL2 expression, is then the highest in plasma cells. However, stage-specificity is not the sole divergent parameter between both models. At all stages, the BCL2 transcription level is also higher for the Igk-BCL2 model. Chromatin marks could also differ since the 3'RR is known to recruit specific epigenetic marks, and the same is true for nuclear location and genome architecture since the 3'RR superenhancer was shown to play a role in long-distance interactions and chromosomal loop extrusion in activated B cells [68,69]. It remains to be determined which of these multiple parameters most strongly impacts the expression of a transgenic or a translocated oncogene.

Supplementary Materials: The following supporting information can be downloaded at: <https://www.mdpi.com/article/10.3390/cancers14215337/s1>, Table S1: List of antibodies used for stainings; Figure S1: Gating strategies for cell cytometry; Figure S2: Heatmap of Top 10 differentially expressed genes between single-cell clusters.

Author Contributions: Conceptualization, M.C. and K.T.; methodology, L.Z., T.M., B.B., A.S., C.C., E.D., C.O., S.L.N., F.M., M.B., M.A., Y.E.M., C.M., and S.D.-P.; software, P.D., J.S.-V., and S.L.; validation, M.C. and K.T.; formal analysis, P.D. and S.L.; investigation, L.Z., T.M., B.B., A.S., C.C., E.D., C.O., S.L.N., F.M., M.B., M.A., Y.E.M., C.M., and S.D.-P.; resources, M.C. and K.T.; data curation, M.C.; writing—original draft preparation, M.C. and L.Z.; writing—review and editing, M.C. and K.T. visualization, M.C. and K.T. supervision, M.C. and K.T.; project administration, M.C. and K.T.; funding acquisition, M.C. and K.T. All authors have read and agreed to the published version of the manuscript.

Funding: This research was funded by grants from Fondation ARC pour la Recherche sur le Cancer (Grant PGA RF20180207070), the Institut National du cancer (INCA 2018-133), the Agence Nationale de la Recherche (ANR, ANR-16-CE15-0019-01/03), the Leukemia Lymphoma Society (TRP 6593-20) and Rennes Métropole. SL was supported by a specific grant from the LabEx IGO program (n° ANR-11-LABX-0016) funded by the «Investment into the Future» French Government program, managed by the National Research Agency (ANR).

Institutional Review Board Statement: The animal study protocol was approved by the Institutional Review Board of Limoges University, with agreement from the Ministry of Research (APAFis 13900, 12 December 2018).

Informed Consent Statement: Not applicable.

Data Availability Statement: All next-generation sequencing data are deposited on G.E.O. (details information can be found in supplementary information).

Acknowledgments: We thank Florence Jouan for technical help and Karine Crozat for helpful discussions. We thank the technological platform BISCEm (Limoges University/UAR 2015 CNRS/US 42 Inserm/CHU Limoges) for animal care. CRIBL and MICMAC are members of the Consortium for the Acceleration of Innovation and Transfer in Lymphoma Field (CALYM) Carnot Institute www.calym.org, accessed on 1 October 2022.

Conflicts of Interest: The authors declare no conflict of interest. The funders had no role in the design of the study; in the collection, analyses, or interpretation of data; in writing the manuscript or decision to publish the results.

References

1. Milpied, P.; Gandhi, A.K.; Cartron, G.; Pasqualucci, L.; Tarte, K.; Nadel, B.; Roulland, S. Follicular Lymphoma Dynamics. *Adv. Immunol.* **2021**, *150*, 43–103. [[CrossRef](#)] [[PubMed](#)]
2. Ruminy, P.; Jardin, F.; Picquenot, J.M.; Gaulard, P.; Parmentier, F.; Buchonnet, G.; Maisonneuve, C.; Tilly, H.; Bastard, C. Two Patterns of Chromosomal Breakpoint Locations on the Immunoglobulin Heavy-Chain Locus in B-Cell Lymphomas with t(3;14)(Q27;Q32): Relevance to Histology. *Oncogene* **2006**, *25*, 4947–4954. [[CrossRef](#)] [[PubMed](#)]
3. Hillion, J.; Mecucci, C.; Aventin, A.; Leroux, D.; Wlodarska, I.; Van Den Berghe, H.; Larsen, C.J. A Variant Translocation t(2;18) in Follicular Lymphoma Involves the 5' End of Bcl-2 and Ig Kappa Light Chain Gene. *Oncogene* **1991**, *6*, 169–172. [[PubMed](#)]
4. Lin, P.; Jetly, R.; Lennon, P.A.; Abruzzo, L.V.; Prajapati, S.; Medeiros, L.J. Translocation (18;22)(Q21;Q11) in B-Cell Lymphomas: A Report of 4 Cases and Review of the Literature. *Hum. Pathol.* **2008**, *39*, 1664–1672. [[CrossRef](#)] [[PubMed](#)]
5. Monni, O.; Joensuu, H.; Franssila, K.; Klefstrom, J.; Alitalo, K.; Knuutila, S. BCL2 Overexpression Associated with Chromosomal Amplification in Diffuse Large B-Cell Lymphoma. *Blood* **1997**, *90*, 1168–1174. [[CrossRef](#)]

6. Raghavan, S.C.; Swanson, P.C.; Wu, X.; Hsieh, C.-L.; Lieber, M.R. A Non-B-DNA Structure at the Bcl-2 Major Breakpoint Region Is Cleaved by the RAG Complex. *Nature* **2004**, *428*, 88–93. [[CrossRef](#)]
7. Pinaud, E.; Marquet, M.; Fiancette, R.; Péron, S.; Vincent-Fabert, C.; Denizot, Y.; Cogné, M. The IgH Locus 3' Regulatory Region: Pulling the Strings from Behind. *Adv. Immunol.* **2011**, *110*, 27–70. [[CrossRef](#)]
8. Cogné, M.; Lansford, R.; Bottaro, A.; Zhang, J.; Gorman, J.; Young, F.; Cheng, H.L.; Alt, F.W. A Class Switch Control Region at the 3' End of the Immunoglobulin Heavy Chain Locus. *Cell* **1994**, *77*, 737–747. [[CrossRef](#)]
9. Rouaud, P.; Vincent-Fabert, C.; Saintamand, A.; Fiancette, R.; Marquet, M.; Robert, I.; Reina-San-Martin, B.; Pinaud, E.; Cogné, M.; Denizot, Y. The IgH 3' Regulatory Region Controls Somatic Hypermutation in Germinal Center B Cells. *J. Exp. Med.* **2013**, *210*, 1501–1507. [[CrossRef](#)]
10. Saintamand, A.; Rouaud, P.; Saad, F.; Rios, G.; Cogné, M.; Denizot, Y. Elucidation of IgH 3' Region Regulatory Role during Class Switch Recombination via Germline Deletion. *Nat. Commun.* **2015**, *6*, 7084. [[CrossRef](#)]
11. Mayer, C.T.; Gazumyan, A.; Kara, E.E.; Gitlin, A.D.; Golijanin, J.; Viant, C.; Pai, J.; Oliveira, T.Y.; Wang, Q.; Escolano, A.; et al. The Microanatomic Segregation of Selection by Apoptosis in the Germinal Center. *Science* **2017**, *358*, 6360. [[CrossRef](#)] [[PubMed](#)]
12. Péron, S.; Laffleur, B.; Denis-Lagache, N.; Cook-Moreau, J.; Tinguely, A.; Delpy, L.; Denizot, Y.; Pinaud, E.; Cogné, M. AID-Driven Deletion Causes Immunoglobulin Heavy Chain Locus Suicide Recombination in B Cells. *Science* **2012**, *336*, 931–934. [[CrossRef](#)] [[PubMed](#)]
13. Milpied, P.; Nadel, B.; Roulland, S. Premalignant Cell Dynamics in Indolent B-Cell Malignancies. *Curr. Opin. Hematol.* **2015**, *22*, 388–396. [[CrossRef](#)]
14. Tellier, J.; Menard, C.; Roulland, S.; Martin, N.; Monvoisin, C.; Chasson, L.; Nadel, B.; Gaulard, P.; Schiff, C.; Tarte, K. Human t(14;18) Positive Germinal Center B Cells: A New Step in Follicular Lymphoma Pathogenesis? *Blood* **2014**, *123*, 3462–3465. [[CrossRef](#)] [[PubMed](#)]
15. Huet, S.; Sujobert, P.; Salles, G. From Genetics to the Clinic: A Translational Perspective on Follicular Lymphoma. *Nat. Rev. Cancer* **2018**, *18*, 224–239. [[CrossRef](#)] [[PubMed](#)]
16. Boice, M.; Salloum, D.; Mourcin, F.; Sanghvi, V.; Amin, R.; Oricchio, E.; Jiang, M.; Mottok, A.; Denis-Lagache, N.; Ciriello, G.; et al. Loss of the HVEM Tumor Suppressor in Lymphoma and Restoration by Modified CAR-T Cells. *Cell* **2016**, *167*, 405–418.e13. [[CrossRef](#)] [[PubMed](#)]
17. Amin, R.; Mourcin, F.; Uhel, F.; Pangault, C.; Ruminy, P.; Dupré, L.; Guirriec, M.; Marchand, T.; Fest, T.; Lamy, T.; et al. DC-SIGN-Expressing Macrophages Trigger Activation of Mannosylated IgM B-Cell Receptor in Follicular Lymphoma. *Blood* **2015**, *126*, 1911–1920. [[CrossRef](#)]
18. Linley, A.; Krysov, S.; Ponzoni, M.; Johnson, P.W.; Packham, G.; Stevenson, F.K. Lectin Binding to Surface Ig Variable Regions Provides a Universal Persistent Activating Signal for Follicular Lymphoma Cells. *Blood* **2015**, *126*, 1902–1910. [[CrossRef](#)]
19. McDonnell, T.J.; Deane, N.; Platt, F.M.; Nunez, G.; Jaeger, U.; McKearn, J.P.; Korsmeyer, S.J. Bcl-2-Immunoglobulin Transgenic Mice Demonstrate Extended B Cell Survival and Follicular Lymphoproliferation. *Cell* **1989**, *57*, 79–88. [[CrossRef](#)]
20. Strasser, A.; Whittingham, S.; Vaux, D.L.; Bath, M.L.; Adams, J.M.; Cory, S.; Harris, A.W. Enforced BCL2 Expression in B-Lymphoid Cells Prolongs Antibody Responses and Elicits Autoimmune Disease. *Proc. Natl. Acad. Sci. USA* **1991**, *88*, 8661–8665. [[CrossRef](#)]
21. Strasser, A.; Harris, A.W.; Bath, M.L.; Cory, S. Novel Primitive Lymphoid Tumours Induced in Transgenic Mice by Cooperation between Myc and Bcl-2. *Nature* **1990**, *348*, 331–333. [[CrossRef](#)] [[PubMed](#)]
22. McDonnell, T.J.; Korsmeyer, S.J. Progression from Lymphoid Hyperplasia to High-Grade Malignant Lymphoma in Mice Transgenic for the t(14; 18). *Nature* **1991**, *349*, 254–256. [[CrossRef](#)] [[PubMed](#)]
23. Ogilvy, S.; Metcalf, D.; Print, C.G.; Bath, M.L.; Harris, A.W.; Adams, J.M. Constitutive Bcl-2 Expression throughout the Hematopoietic Compartment Affects Multiple Lineages and Enhances Progenitor Cell Survival. *Proc. Natl. Acad. Sci. USA* **1999**, *96*, 14943–14948. [[CrossRef](#)] [[PubMed](#)]
24. Egle, A.; Harris, A.W.; Bath, M.L.; O'Reilly, L.; Cory, S. VavP-Bcl2 Transgenic Mice Develop Follicular Lymphoma Preceded by Germinal Center Hyperplasia. *Blood* **2004**, *103*, 2276–2283. [[CrossRef](#)] [[PubMed](#)]
25. Saito, M.; Novak, U.; Piovan, E.; Basso, K.; Sumazin, P.; Schneider, C.; Crespo, M.; Shen, Q.; Bhagat, G.; Califano, A.; et al. BCL6 Suppression of BCL2 via Miz1 and Its Disruption in Diffuse Large B Cell Lymphoma. *Proc. Natl. Acad. Sci. USA* **2009**, *106*, 11294–11299. [[CrossRef](#)]
26. Le Noir, S.; Bonaud, A.; Hervé, B.; Baylet, A.; Boyer, F.; Lecardeur, S.; Oruc, Z.; Sirac, C.; Cogné, M. IgH 3' Regulatory Region Increases Ectopic Class Switch Recombination. *PLoS Genet.* **2021**, *17*, e1009288. [[CrossRef](#)]
27. Zhang, C.; Li, R.; Li, Y.; Song, C.; Liu, Z.; Zhang, Y.; Xu, Z.; Zhuang, R.; Yi, J.; Yang, A.; et al. Establishment of Reverse Direct ELISA and Its Application in Screening High-Affinity Monoclonal Antibodies. *Hybridoma* **2012**, *31*, 284–288. [[CrossRef](#)]
28. Javaugue, V.; Pascal, V.; Bender, S.; Nasraddine, S.; Dargelos, M.; Alizadeh, M.; Saintamand, A.; Filloux, M.; Derouault, P.; Bouyer, S.; et al. RNA-Based Immunoglobulin Repertoire Sequencing Is a New Tool for the Management of Monoclonal Gammopathy of Renal (Kidney) Significance. *Kidney Int.* **2021**, *101*, 331–337. [[CrossRef](#)]
29. Magoč, T.; Salzberg, S.L. FLASH: Fast Length Adjustment of Short Reads to Improve Genome Assemblies. *Bioinformatics* **2011**, *27*, 2957–2963. [[CrossRef](#)]
30. Li, S.; Lefranc, M.-P.; Miles, J.J.; Alamyar, E.; Giudicelli, V.; Duroux, P.; Freeman, J.D.; Corbin, V.D.A.; Scheerlinck, J.-P.; Frohman, M.A.; et al. IMGT/HighV QUEST Paradigm for T Cell Receptor IMGT Clonotype Diversity and next Generation Repertoire Immunoprofiling. *Nat. Commun.* **2013**, *4*, 2333. [[CrossRef](#)]

31. Anders, S.; Huber, W. Differential Expression Analysis for Sequence Count Data. *Genome Biol.* **2010**, *11*, R106. [[CrossRef](#)] [[PubMed](#)]
32. Stuart, T.; Butler, A.; Hoffman, P.; Hafemeister, C.; Papalexi, E.; Mauck, W.M.; Hao, Y.; Stoeckius, M.; Smibert, P.; Satija, R. Comprehensive Integration of Single-Cell Data. *Cell* **2019**, *177*, 1888–1902.e21. [[CrossRef](#)] [[PubMed](#)]
33. Hafemeister, C.; Satija, R. Normalization and Variance Stabilization of Single-Cell RNA-Seq Data Using Regularized Negative Binomial Regression. *Genome Biol.* **2019**, *20*, 296. [[CrossRef](#)] [[PubMed](#)]
34. Butler, A.; Hoffman, P.; Smibert, P.; Papalexi, E.; Satija, R. Integrating Single-Cell Transcriptomic Data across Different Conditions, Technologies, and Species. *Nat. Biotechnol.* **2018**, *36*, 411–420. [[CrossRef](#)]
35. Kowalczyk, M.S.; Tirosh, I.; Heckl, D.; Rao, T.N.; Dixit, A.; Haas, B.J.; Schneider, R.K.; Wagers, A.J.; Ebert, B.L.; Regev, A. Single-Cell RNA-Seq Reveals Changes in Cell Cycle and Differentiation Programs upon Aging of Hematopoietic Stem Cells. *Genome Res.* **2015**, *25*, 1860–1872. [[CrossRef](#)]
36. Martin, O.A.; Garot, A.; Noir, S.L.; Aldigier, J.-C.; Cogné, M.; Pinaud, E.; Boyer, F. Detecting Rare AID-Induced Mutations in B-Lineage Oncogenes from High-Throughput Sequencing Data Using the Detection of Minor Variants by Error Correction Method. *J. Immunol.* **2018**, *201*, 950–956. [[CrossRef](#)]
37. Chevrier, S.; Genton, C.; Kallies, A.; Karnowski, A.; Otten, L.A.; Malissen, B.; Malissen, M.; Botto, M.; Corcoran, L.M.; Nutt, S.L.; et al. CD93 Is Required for Maintenance of Antibody Secretion and Persistence of Plasma Cells in the Bone Marrow Niche. *Proc. Natl. Acad. Sci. USA* **2009**, *106*, 3895–3900. [[CrossRef](#)]
38. Smith, K.G.; Light, A.; O'Reilly, L.A.; Ang, S.M.; Strasser, A.; Tarlinton, D. Bcl-2 Transgene Expression Inhibits Apoptosis in the Germinal Center and Reveals Differences in the Selection of Memory B Cells and Bone Marrow Antibody-Forming Cells. *J. Exp. Med.* **2000**, *191*, 475–484. [[CrossRef](#)]
39. Golay, J.; Broccoli, V.; Lamorte, G.; Bifulco, C.; Parravicini, C.; Pizzey, A.; Thomas, N.S.; Delia, D.; Ferrauti, P.; Vitolo, D.; et al. The A-Myb Transcription Factor Is a Marker of Centробlasts in Vivo. *J. Immunol.* **1998**, *160*, 2786–2793.
40. Richter, K.; Burch, L.; Chao, F.; Henke, D.; Jiang, C.; Daly, J.; Zhao, M.-L.; Kissling, G.; Diaz, M. Altered Pattern of Immunoglobulin Hypermutation in Mice Deficient in Slip-GC Protein. *J. Biol. Chem.* **2012**, *287*, 31856–31865. [[CrossRef](#)]
41. Laidlaw, B.J.; Schmidt, T.H.; Green, J.A.; Allen, C.D.C.; Okada, T.; Cyster, J.G. The Eph-Related Tyrosine Kinase Ligand Ephrin-B1 Marks Germinal Center and Memory Precursor B Cells. *J. Exp. Med.* **2017**, *214*, 639–649. [[CrossRef](#)]
42. Brescia, P.; Schneider, C.; Holmes, A.B.; Shen, Q.; Hussein, S.; Pasqualucci, L.; Basso, K.; Dalla-Favera, R. MEF2B Instructs Germinal Center Development and Acts as an Oncogene in B Cell Lymphomagenesis. *Cancer Cell* **2018**, *34*, 453–465.e9. [[CrossRef](#)] [[PubMed](#)]
43. Todd, D.J.; McHeyzer-Williams, L.J.; Kowal, C.; Lee, A.-H.; Volpe, B.T.; Diamond, B.; McHeyzer-Williams, M.G.; Glimcher, L.H. XBP1 Governs Late Events in Plasma Cell Differentiation and Is Not Required for Antigen-Specific Memory B Cell Development. *J. Exp. Med.* **2009**, *206*, 2151–2159. [[CrossRef](#)] [[PubMed](#)]
44. O'Connor, B.P.; Raman, V.S.; Erickson, L.D.; Cook, W.J.; Weaver, L.K.; Ahonen, C.; Lin, L.-L.; Mantchev, G.T.; Bram, R.J.; Noelle, R.J. BCMA Is Essential for the Survival of Long-Lived Bone Marrow Plasma Cells. *J. Exp. Med.* **2004**, *199*, 91–98. [[CrossRef](#)] [[PubMed](#)]
45. Kassambara, A.; Herviou, L.; Ovejero, S.; Jourdan, M.; Thibaut, C.; Vikova, V.; Pasero, P.; Elemento, O.; Moreaux, J. RNA-Sequencing Data-Driven Dissection of Human Plasma Cell Differentiation Reveals New Potential Transcription Regulators. *Leukemia* **2021**, *35*, 1451–1462. [[CrossRef](#)] [[PubMed](#)]
46. Gehrie, E.; Van der Touw, W.; Bromberg, J.S.; Ochando, J.C. Plasmacytoid Dendritic Cells in Tolerance. *Methods Mol. Biol.* **2011**, *677*, 127–147. [[CrossRef](#)] [[PubMed](#)]
47. Touzeau, C.; Maciag, P.; Amiot, M.; Moreau, P. Targeting Bcl-2 for the Treatment of Multiple Myeloma. *Leukemia* **2018**, *32*, 1899–1907. [[CrossRef](#)] [[PubMed](#)]
48. Gupta, V.A.; Barwick, B.G.; Matulis, S.M.; Shirasaki, R.; Jaye, D.L.; Keats, J.J.; Oberlton, B.; Joseph, N.S.; Hofmeister, C.C.; Heffner, L.T.; et al. Venetoclax Sensitivity in Multiple Myeloma Is Associated with B-Cell Gene Expression. *Blood* **2021**, *137*, 3604–3615. [[CrossRef](#)]
49. Hervás-Salcedo, R.; Martín-Antonio, B. A Journey through the Inter-Cellular Interactions in the Bone Marrow in Multiple Myeloma: Implications for the Next Generation of Treatments. *Cancers* **2022**, *14*, 3796. [[CrossRef](#)]
50. Roulland, S.; Faroudi, M.; Mamessier, E.; Sungalee, S.; Salles, G.; Nadel, B. Early Steps of Follicular Lymphoma Pathogenesis. *Adv. Immunol.* **2011**, *111*, 1–46. [[CrossRef](#)]
51. Sungalee, S.; Mamessier, E.; Morgado, E.; Grégoire, E.; Brohawn, P.Z.; Morehouse, C.A.; Jouve, N.; Monvoisin, C.; Menard, C.; Debros, G.; et al. Germinal Center Reentries of BCL2-Overexpressing B Cells Drive Follicular Lymphoma Progression. *J. Clin. Invest.* **2014**, *124*, 5337–5351. [[CrossRef](#)] [[PubMed](#)]
52. Vogelsberg, A.; Steinhilber, J.; Mankel, B.; Federmann, B.; Schmidt, J.; Montes-Mojarro, I.A.; Hüttl, K.; Rodriguez-Pinilla, M.; Baskaran, P.; Nahnsen, S.; et al. Genetic Evolution of in Situ Follicular Neoplasia to Aggressive B-Cell Lymphoma of Germinal Center Subtype. *Haematologica* **2021**, *106*, 2673–2681. [[CrossRef](#)] [[PubMed](#)]
53. Lu, X.; Fernando, T.M.; Lossos, C.; Yusufova, N.; Liu, F.; Fontán, L.; Durant, M.; Geng, H.; Melnick, J.; Luo, Y.; et al. PRMT5 Interacts with the BCL6 Oncoprotein and Is Required for Germinal Center Formation and Lymphoma Cell Survival. *Blood* **2018**, *132*, 2026–2039. [[CrossRef](#)]

54. Dominguez, P.M.; Ghamlouch, H.; Rosikiewicz, W.; Kumar, P.; Béguelin, W.; Fontán, L.; Rivas, M.A.; Pawlikowska, P.; Armand, M.; Mouly, E.; et al. TET2 Deficiency Causes Germinal Center Hyperplasia, Impairs Plasma Cell Differentiation, and Promotes B-Cell Lymphomagenesis. *Cancer Discov.* **2018**, *8*, 1632–1653. [[CrossRef](#)]
55. Rivas, M.A.; Meydan, C.; Chin, C.R.; Challman, M.F.; Kim, D.; Bhinder, B.; Kloetgen, A.; Viny, A.D.; Teater, M.R.; McNally, D.R.; et al. Smc3 Dosage Regulates B Cell Transit through Germinal Centers and Restricts Their Malignant Transformation. *Nat. Immunol.* **2021**, *22*, 240–253. [[CrossRef](#)] [[PubMed](#)]
56. Béguelin, W.; Teater, M.; Meydan, C.; Hoehn, K.B.; Phillip, J.M.; Soshnev, A.A.; Venturutti, L.; Rivas, M.A.; Calvo-Fernández, M.T.; Gutierrez, J.; et al. Mutant EZH2 Induces a Pre-Malignant Lymphoma Niche by Reprogramming the Immune Response. *Cancer Cell* **2020**, *37*, 655–673.e11. [[CrossRef](#)]
57. Toellner, K.-M.; Jenkinson, W.E.; Taylor, D.R.; Khan, M.; Sze, D.M.-Y.; Sansom, D.M.; Vinuesa, C.G.; MacLennan, I.C.M. Low-Level Hypermutation in T Cell-Independent Germinal Centers Compared with High Mutation Rates Associated with T Cell-Dependent Germinal Centers. *J. Exp. Med.* **2002**, *195*, 383–389. [[CrossRef](#)]
58. Szymanowska, N.; Klapper, W.; Gesk, S.; Küppers, R.; Martín-Subero, J.I.; Siebert, R. BCL2 and BCL3 Are Recurrent Translocation Partners of the IGH Locus. *Cancer Genet. Cytogenet.* **2008**, *186*, 110–114. [[CrossRef](#)]
59. Peperzak, V.; Vikström, I.; Walker, J.; Glaser, S.P.; LePage, M.; Coquery, C.M.; Erickson, L.D.; Fairfax, K.; Mackay, F.; Strasser, A.; et al. Mcl-1 Is Essential for the Survival of Plasma Cells. *Nat. Immunol.* **2013**, *14*, 290–297. [[CrossRef](#)]
60. Onnis, A.; Cianfanelli, V.; Cassioli, C.; Samardzic, D.; Pelicci, P.G.; Cecconi, F.; Baldari, C.T. The Pro-Oxidant Adaptor P66SHC Promotes B Cell Mitophagy by Disrupting Mitochondrial Integrity and Recruiting LC3-II. *Autophagy* **2018**, *14*, 2117–2138. [[CrossRef](#)]
61. Onishi, M.; Yamano, K.; Sato, M.; Matsuda, N.; Okamoto, K. Molecular Mechanisms and Physiological Functions of Mitophagy. *EMBO J.* **2021**, *40*, e104705. [[CrossRef](#)] [[PubMed](#)]
62. Murai, M.; Toyota, M.; Satoh, A.; Suzuki, H.; Akino, K.; Mita, H.; Sasaki, Y.; Ishida, T.; Shen, L.; Garcia-Manero, G.; et al. Aberrant DNA Methylation Associated with Silencing BNIP3 Gene Expression in Haematopoietic Tumours. *Br. J. Cancer* **2005**, *92*, 1165–1172. [[CrossRef](#)] [[PubMed](#)]
63. Ma, M.C.J.; Tadros, S.; Bouska, A.; Heavican, T.; Yang, H.; Deng, Q.; Moore, D.; Akhter, A.; Hartert, K.; Jain, N.; et al. Subtype-Specific and Co-Occurring Genetic Alterations in B-Cell Non-Hodgkin Lymphoma. *Haematologica* **2022**, *107*, 690–701. [[CrossRef](#)]
64. Michaelson, J.S.; Singh, M.; Birshstein, B.K. B Cell Lineage-Specific Activator Protein (BSAP). A Player at Multiple Stages of B Cell Development. *J. Immunol.* **1996**, *156*, 2349–2351.
65. Arulampalam, V.; Grant, P.A.; Samuelsson, A.; Lendahl, U.; Pettersson, S. Lipopolysaccharide-Dependent Transactivation of the Temporally Regulated Immunoglobulin Heavy Chain 3' Enhancer. *Eur. J. Immunol.* **1994**, *24*, 1671–1677. [[CrossRef](#)]
66. Neurath, M.F.; Max, E.E.; Strober, W. Pax5 (BSAP) Regulates the Murine Immunoglobulin 3' Alpha Enhancer by Suppressing Binding of NF-Alpha P, a Protein That Controls Heavy Chain Transcription. *Proc. Natl. Acad. Sci. USA* **1995**, *92*, 5336–5340. [[CrossRef](#)]
67. Muto, A.; Hoshino, H.; Madisen, L.; Yanai, N.; Obinata, M.; Karasuyama, H.; Hayashi, N.; Nakauchi, H.; Yamamoto, M.; Groudine, M.; et al. Identification of Bach2 as a B-Cell-Specific Partner for Small Maf Proteins That Negatively Regulate the Immunoglobulin Heavy Chain Gene 3' Enhancer. *EMBO J.* **1998**, *17*, 5734–5743. [[CrossRef](#)] [[PubMed](#)]
68. Zhang, X.; Zhang, Y.; Ba, Z.; Kyritsis, N.; Casellas, R.; Alt, F.W. Fundamental Roles of Chromatin Loop Extrusion in Antibody Class Switching. *Nature* **2019**, *575*, 385–389. [[CrossRef](#)]
69. Wuerffel, R.; Wang, L.; Grigera, F.; Manis, J.; Selsing, E.; Perlot, T.; Alt, F.W.; Cogne, M.; Pinaud, E.; Kenter, A.L. S-S Synapsis during Class Switch Recombination Is Promoted by Distantly Located Transcriptional Elements and Activation-Induced Deaminase. *Immunity* **2007**, *27*, 711–722. [[CrossRef](#)] [[PubMed](#)]